J. Fluid Mech. (2004), *vol.* 503, *pp.* 125–160.
DOI: 10.1017/S0022112003007596 Printed in the United Kingdom

Relative dispersion in isotropic turbulence. Part 2. A new stochastic model with Reynolds-number dependence

By MICHAEL S. BORGAS[1] AND P. K. YEUNG[2]

[1]CSIRO Atmospheric Research, Private Bag no. 1, Aspendale, VIC 3195, Australia
michael.borgas@csiro.au

[2]School of Aerospace Engineering, Georgia Institute of Technology, Atlanta, GA 30332, USA
yeung@peach.ae.gatech.edu

(Received 8 August 2002 and in revised form 22 September 2003)

A new model for Lagrangian particle-pair separation in turbulent flows is developed and compared with data from direct numerical simulations (DNS) of isotropic turbulence. The model formulation emphasizes (i) non-Gaussian behaviour in Eulerian and Lagrangian statistics, (ii) the occurrence of large separation velocities, (iii) the role of straining and streaming flow structure as recognized in kinematic simulations of turbulence, and (iv) the role of conditionally averaged accelerations in stochastic modelling of turbulent relative dispersion. Previous stochastic models of relative dispersion have produced unrealistic behaviour, particularly in the dissipation subrange where viscous effects are important, which have led to questions on the adequacy of stochastic modelling. However, this failure can now be recognized as inadequate detail in formulation, which is explained and rectified in this paper. The model is quasi-one-dimensional in nature, and is focused on the statistics of particle-pair separation distance and its rate of change, referred to as the separation speed. Detailed comparisons are presented at several Reynolds numbers using the DNS database reported in a companion paper (Part 1). Up to fourth-order moments for these quantities are examined, as well as the separation-distance probability density function, which is discussed in the context of recent claims of Richardson scaling in the literature. The model is able to account for the spatial representation of straining regions as well as incompressibility of the flow, and is shown to reproduce strong non-Gaussianity and intermittency in the Lagrangian separation statistics observed in DNS. Comparisons with recent physical experiments are also remarkably consistent. This work demonstrates that stochastic models when properly formulated are effective and efficient representations of the dispersion process and this general class of models therefore possess great utility for calculations of both one-particle and two-particle dispersion. The techniques developed in this paper will facilitate such general model development.

1. Introduction

The rate at which pairs of marked particles move apart in turbulent flows plays a fundamental role in many fluid flow problems, including concentration fluctuations of transported passive tracers (Batchelor 1952; Durbin 1980; Sawford 1985, 2001; Thomson 1990; Borgas & Sawford 1996), encounter rates for droplets and swimming micro-organisms (Lewis & Pedley 2000), and the deformation of material interfaces

(Girimaji & Pope 1990). Knowledge of the statistics of separation rate in time is especially important in environmental applications, such as pollutant dispersion in the atmosphere (Luhar, Hibberd & Borgas 2000; Franzese & Borgas 2002). In practice, say for convective turbulence during daytime conditions, this usually involves complex turbulent flows at high Reynolds number, with a wide range of time and length scales. Such parameter and flow regimes are beyond the range of current computation, thus environmental applications require the use of models. The class of stochastic models, which are widely applied in pollutant dispersion, is examined in detail here.

We can simplify matters by noting that the separation rate at any instant depends mainly on local flow conditions encountered by fluid particle pairs when they are relatively close together. In particular, when the separation distances are small (of the order of the Kolmogorov length scale, η) the separation process will resemble that occurring in the idealized case of isotropic turbulence, and will be highly sensitive to the flow structure expressed by the Eulerian statistics of velocity gradients and two-point velocity differences. On the other hand, when the separations become large (comparable to the integral length scale, L) the motions of separate particles become nearly independent and easier to describe. In other words, the fundamental phenomena of relative dispersion are small scale and generally at high Reynolds number. The expectation of (at least approximate) small-scale universality then suggests that a generic description may be possible in terms of appropriately scaled variables independent of details of the large scales.

This paper is Part 2 of a coordinated effort to validate the stochastic model description of relative dispersion in homogeneous isotropic turbulence, with the aid of direct numerical simulation (DNS) data at several different Reynolds numbers (Yeung & Borgas 2004, hereinafter referred to a Part 1). Special attention is paid to the pair separation process as described by its statistics and rates of growth. Although the flow configuration considered here is one of the simplest in turbulence, knowledge of quantitative details about the separation process is still limited. The best source of information is from DNS with Lagrangian particle tracking (Yeung & Pope 1989; Yeung 1994; Part 1). Some information is also available from the laboratory experiments of Ott & Mann (2000) where advanced optical techniques are used to follow particle trajectories. The advantage of DNS is the degree of detail available and with increasing computer power, the simulations now provide reliable data over a substantial range of Reynolds numbers. We use recent DNS results to evaluate and suggest improvements for the new stochastic model applied at different Reynolds numbers. Substantial attention is paid to the relatively strong Reynolds-number dependence known for Lagrangian statistics (see, e.g. Sawford 1991; Pope 1994; Yeung 2002).

Most stochastic models for particle-pair dispersion in the literature (Thomson 1990; Borgas & Sawford 1994*a*; Pedrizzetti & Novikov 1994; Heppe 1998; Kurbanmuradov 1995; Kurbanmuradov & Sabelfeld 1995; Pedrizzetti 1999; Reynolds 1999) have used a Langevin-type equation for particle velocities. These models assume that particle accelerations have negligible memory, which implies that Lagrangian position and velocity can be described by treating the latter as a Markov process (Borgas & Sawford 1994*b*; Sawford & Borgas 1994). However, the neglect of viscous memory effects in these models makes them inherently incapable of describing Reynolds-number effects in a quantitative manner. One effect of viscosity is very strong non-Gaussian particle-pair separations, which is apparently captured well by an alternative approach, namely *kinematic simulations* (Fung *et al.* 1992; Malik & Vassilicos 1999). In kinematic simulations (KS), the instantaneous velocity field is modelled by a superposition of random Fourier modes chosen to satisfy incompressibility and with spectral and

spatial structure similar to real turbulence. Past difficulties in stochastic modelling have been highlighted in some papers which advocate kinematic simulations as a better technique (Malik & Vassilicos 1999; Flohr & Vassilicos 2000). However, here we show that, with the aid of DNS data, these limitations are successfully overcome by a new model that explicitly accounts for viscous dissipation range effects and by accounting for an anomalously high probability of large-amplitude separation velocities.

The emphasis of this paper is to demonstrate the feasibility of stochastic model representation, not necessarily its optimality. The optimal use of stochastic models is always thought to reside in the inertial-range of scales for larger and larger Reynolds number. However, the need for validation of models forces the finite-Reynolds-number dissipation-range focus. It is assumed that reliability of the demanding viscous-range modelling will also validate modelling in the extrapolated inertial ranges. This study therefore underpins the validity of stochastic models. Some of the techniques introduced also have more general applications for stochastic models (quadratic-form closures in particular), and some important insights into the Lagrangian separation process emerge.

New applications will be developed from the framework established in this paper, for example models for the decay of scalar variance in turbulent flows (Durbin 1982; Thomson 1990; Borgas & Sawford 1996). These applications require either the inclusion of explicit molecular diffusion effects, extension to more complex inhomogeneous flows, or extrapolation to the inertial-range of scales (for atmospheric applications), all of which remain as future work. However, the framework successfully developed in this paper can be adapted for more general purposes, including practical applications.

In § 2, we briefly describe the mathematical background for relative dispersion, and the rationale for a stochastic model solely for the separation distance (l) between fluid particle pairs. Our focus is on l, and its rate of change (here called the separation speed), instead of the orientation of the separation vector (Yeung & Borgas 1998). In § 3, we discuss Eulerian quantities that carry information on the local flow topology relevant to the model formulation. Of particular importance is the Eulerian mean acceleration conditioned on the separation speed at specified spatial separation distance (Borgas & Yeung 1998), which is an unclosed term in the transport equation for the probability density function (p.d.f.) for two-point velocity differences. Accurate yet simple parameterizations of these quantities are emphasized, with some of the details left to the Appendix. In § 4, we show how Langevin-stochastic models for Lagrangian velocity, based on fluid-particle accelerations, are modified to account for small-scale viscous effects. Solutions of the model are examined with emphasis on characteristics of non-Gaussianity and intermittency. In § 5, we consider issues of numerical implementation and statistical sampling. Detailed comparisons between the model and DNS are presented in § 6, with generally good agreement (with tuned parameters to fit separation mean and variance) at three different Reynolds numbers up to the highest for which detailed information is currently available. Separate subsections are devoted to moments of the separation distance, moments of the separation speed, and the p.d.f. of separation distance. It should be noted that higher moments, the separation speed statistics, and the separation p.d.f., all form 'independent' tests of the tuned model. Comparison of separation-distance p.d.f.s with recent oscillating-grid turbulence experiments also shows remarkable agreement. Finally, in § 7, we summarize the conclusions and discuss implications for dispersion modelling in more practical flows with greater complexities.

2. Background

Relative dispersion is a classic problem in turbulence theory (Richardson 1926; Batchelor 1952; reviewed by Sawford 2001). Consider two marked particles at positions $\boldsymbol{x}^{(1)}(t)$ and $\boldsymbol{x}^{(2)}(t)$, with the separation vector defined as

$$\boldsymbol{l}(t) = \boldsymbol{x}^{(2)}(t) - \boldsymbol{x}^{(1)}(t). \tag{1}$$

As in Part 1, our main task is to determine how quickly the separation vector between fluid particle pairs grows (on average) with time from a specified initial separation distance $l_0 \equiv \sqrt{l_i l_i}$ at $t = 0$. We consider $\boldsymbol{l}(t)$ as a vector stochastic process, with the p.d.f. denoted by $P(\boldsymbol{l}, t)$. Statistical moments are of primary interest. In particular, the second moment gives the mean-squared separation as

$$\langle l^2 \rangle = \langle l_i l_i \rangle = \int l^2 P(\boldsymbol{l})\, \mathrm{d}^3\boldsymbol{l} = 4\pi \int_0^\infty l^4 q(l)\, \mathrm{d}l, \tag{2}$$

where in the last equality sign we have integrated over the surface of a sphere of radius $l = \sqrt{l_i l_i}$, and q is the p.d.f. for scalar separation l. For separation scales much larger than $\eta = (\nu^3/\overline{\epsilon})^{1/4}$ (where $\overline{\epsilon}$ is the energy dissipation rate and ν is the kinematic viscosity), the evolution of $\langle l^2 \rangle$ should be independent of viscosity. Similarly, for scale sizes much smaller than L, the details of the large-scale motion should be unimportant. In the regime where both of these conditions hold, the classical inertial-range prediction (Richardson 1926; Obukhov 1941*a*, *b*) is

$$\langle l^2 \rangle \sim g \overline{\epsilon} t^3 \quad (\eta \ll l_0 \ll \sqrt{\langle l^2 \rangle} \ll L), \tag{3}$$

where g is a non-dimensional coefficient known as Richardson's constant and t is the elapsed time from when the pair of particles were practically next to each other. The applicability of this 'law' depends on several critical conditions: neglect of viscous effects; neglect of large-scale advection effects (which just move the particle pair in bulk together); and loss of memory of the specific initial separation. The time scale for the memory loss is $t_0 = (l_0^2/\overline{\epsilon})^{1/3}$. Unfortunately, observations of Richardson scaling are very difficult in both numerical simulations and laboratory experiments because of their limited Reynolds-number range. The assumptions involved are believed to hold best in the atmosphere with its vast range of scale sizes; however, atmospheric measurements are often noisy and affected by the uncontrollability of conditions in the field. As a result, the value of g is very uncertain, with estimates as low as 0.01 and as high as 4 in the literature (see Sawford 2001).

Because detailed comparisons with DNS of the type reported in this paper are only possible at modest Reynolds numbers, for practical purposes, say for applications in the atmosphere, we cannot avoid the need to make rather tenuous extrapolations to a higher-Reynolds-number range. The key to success for such extrapolations rests directly on the precision with which the small-scale properties of relative dispersion can be described, and whether some type of similarity law can be established. The nature of Reynolds-number dependence is therefore crucial in this investigation.

2.1. *Separation velocity and stochastic models*

The instantaneous rate of separation defines the separation velocity, i.e.

$$\frac{\mathrm{d}\boldsymbol{l}}{\mathrm{d}t} = \boldsymbol{u}^{(r)}, \tag{4}$$

where $\boldsymbol{u}^{(r)} = \boldsymbol{u}^{(2)} - \boldsymbol{u}^{(1)}$ is the relative velocity between two fluid particles at time t. Different approaches for the calculation of relative dispersion can be distinguished

by different prescriptions for the statistics of this relative velocity. In kinematic simulations, Lagrangian statistics are obtained by tracking the motion of fluid particles in a modelled velocity flow field with specified Eulerian characteristics. Alternatively, stochastic models generate sample fluid-particle velocities as random processes, which can be manipulated to be consistent with prescribed Eulerian statistics of the flow. In contrast, direct numerical simulations produce 'exact' Eulerian fields at each time instant, which allows the positions of both particles in each pair to be continuously tracked in time. Notwithstanding its own limitations (especially in the Reynolds number), DNS can be regarded as the most accurate approach, and has indeed provided evidence (Yeung 1994; Part 1) of remarkably strong non-Gaussianity in particle pair separation, which we attempt to model in this paper.

Some of the basic kinematic results for relative dispersion are easy to derive (Borgas & Sawford 1991). These include the separation covariance tensor

$$\langle l_i l_j \rangle = l_{0i} l_{0j} + \int_0^t \int_0^t \left\langle u_i^{(r)}(t_1) u_j^{(r)}(t_2) \right\rangle \mathrm{d}t_1 \, \mathrm{d}t_2 \tag{5}$$

where the velocity covariance inside the integral can be expressed in terms of the relative acceleration $\boldsymbol{a}^{(r)} = \boldsymbol{a}^{(2)} - \boldsymbol{a}^{(1)}$, as

$$\left\langle u_i^{(r)}(t_1) u_j^{(r)}(t_2) \right\rangle = \left\langle u_i^{(r)}(0) u_j^{(r)}(0) \right\rangle + \int_0^{t_1} \int_0^{t_2} \left\langle a_i^{(r)}(t_1') a_j^{(r)}(t_2') \right\rangle \mathrm{d}t_1' \, \mathrm{d}t_2'. \tag{6}$$

As mentioned in § 1, in this paper we attempt to account for viscous effects in dispersion via improved representations of Lagrangian accelerations allowing for finite correlation times. The ultimate predictive target in the modelling is the behaviour of the separation distance (including its higher-order moments), rather than the details of the velocity or the acceleration. Nevertheless, it is encouraging to find that (see § 6) Lagrangian velocity statistics are also reasonably well predicted. Even the accelerations, which are, strictly speaking, unphysical when modelled using the commonly applied Langevin equation for velocity, are in some aspects qualitatively well represented. This success is in part achieved by using the Eulerian conditional acceleration (Borgas & Yeung 1998) as part of the model input.

The stochastic model we use is that of a diffusion process in velocity-separation phase space: namely the Langevin equation for velocity evolution

$$\begin{aligned} \mathrm{d}u_i^{(r)} &= A_i\left(\boldsymbol{u}^{(r)}, \boldsymbol{l}, t\right) \mathrm{d}t + \mu \, \mathrm{d}W_i, \\ \mathrm{d}l_i &= u_i^{(r)} \, \mathrm{d}t, \end{aligned} \tag{7}$$

where $\mathrm{d}W_i \equiv W_i(t + \mathrm{d}t) - W_i(t)$ is a standard Wiener process increment with the properties

$$\langle \mathrm{d}W_i \rangle = 0, \quad \langle \mathrm{d}W_i(t) \, \mathrm{d}W_j(t) \rangle = \delta_{ij} \, \mathrm{d}t, \quad \langle \mathrm{d}W_i(t) \, \mathrm{d}W_j(t') \rangle = 0 \quad (t \neq t'). \tag{8}$$

These equations define a Markov model with continuous trajectories in phase space (Sawford & Borgas 1994), with unknown drift term $\boldsymbol{A}$ (a function of both velocity and separation), and unknown coefficient μ for the noise term. In atmospheric science stochastic models are derived using Eulerian flow-field statistics in a systematic manner (Thomson 1987, 1990). That approach is also followed here, facilitated by a simplification, and with a focus on dissipation-range viscous effects to allow comparisons with DNS.

2.2. *Quasi-one-dimensional model*

Instead of modelling the full separation vector ($\boldsymbol{l}$) it is easier to focus on its magnitude, i.e. the separation distance (l). This reduces our modelling task to that for a quasi-one-dimensional process (Durbin 1980; Durbin 1982; Kurbanmuradov 1997; Borgas & Yeung 1998). This strategy also has the advantage of avoiding a non-uniqueness problem discussed in the literature (e.g. Thomson 1990; Borgas & Yeung 1998) for the relationship between Eulerian velocity p.d.f. and conditional accelerations. The important variables are now just the instantaneous separation distance and its rate of change

$$l = \sqrt{l_i l_i}, \quad u = \frac{\mathrm{d}l}{\mathrm{d}t}. \tag{9}$$

(Note that the notation u is chosen for simplicity here; it corresponds to u_r in Part 1.) We refer to the latter as the separation speed. The corresponding quantity in the Eulerian frame is the 'longitudinal' two-point velocity difference, e.g.

$$\Delta_r u \equiv u_1(x_1 + l, x_2, x_3) - u_1(x_1, x_2, x_3), \tag{10}$$

where the spatial increment is taken in the same direction as the velocity component considered. The moments of $\Delta_r u$ are the Eulerian longitudinal structure functions, which are relatively well known. Some of the relevant scaling properties are

$$\langle (\Delta_r u)^2 \rangle \sim \begin{cases} \langle s^2 \rangle l^2, & l \ll \eta, \\ C_{Kol}(\overline{\epsilon} l)^{2/3}, & \eta \ll l \ll L, \\ 2\sigma_u^2, & l \gg L, \end{cases} \tag{11}$$

where $\langle s^2 \rangle = \langle (\partial u_1/\partial x_1)^2 \rangle$ is given by $\overline{\epsilon}/15\nu$ (assuming local isotropy), C_{Kol} is the Kolmogorov constant in the second-order structure function, and σ_u is the one-particle root-mean-square (r.m.s) component velocity. The value of C_{Kol} inferred from experiments (Sreenivasan 1995) and numerical simulations (Yeung & Zhou 1997) is about 2.1. The different scaling ranges in (11) may be characterized, respectively, as the dissipation range, the inertial range and the energy-containing range. An estimate for the large-eddy scale size L based on known results for the scaling of the dissipation rate (Sreenivasan 1998) can be written as $\sigma_u^3/\overline{\epsilon}$ where a numerical coefficient of order unity is absorbed in the definition. The specification of structure functions in space corresponds to the spectral information used in kinematic simulations (Malik & Vassilicos 1999).

It is important that the model satisfies homogeneity and incompressibility which apply in the numerical simulations. From the definition of $\Delta_r u$ in (10) above, it follows that in homogeneous turbulence $\langle \Delta_r u \rangle = 0$ for all values of r. This condition also represents incompressibility because it implies that there is no mean net mass flow across any arbitrary cross-sectional plane in the solution domain. In general, the local mass flow induced by a non-zero random instantaneous longitudinal velocity $\Delta_r u$ may be considered to be balanced by appropriate velocity components in the plane orthogonal to the vector $\boldsymbol{r}$. Because of the quasi-one-dimensional nature of our model, these velocities in the orthogonal plane do not require modelling. Nevertheless, we stress that incompressibility is a self-consistent property of stochastic models, provided that the model yields a zero mean for the Eulerian two-point velocity difference.

Higher-order moments of $\Delta_r u$ are also of interest. In particular Kolmogorov's 4/5th law (Monin & Yaglom 1975) for the third-order structure function says

$$\langle(\Delta_r u)^3\rangle \sim \begin{cases} \langle s^3\rangle l^3, & l \ll \eta, \\ -\frac{4}{5}\overline{\epsilon} l, & \eta \ll l \ll L. \end{cases} \tag{12}$$

Moments at yet higher orders are also known (Anselmet *et al.* 1984; Sreenivasan & Antonia 1997; Pope 2000), but here we will use only the first four as assumed Eulerian empirical input for constructing models for Lagrangian trajectories in non-Gaussian flow fields. In doing so, we also successfully avoid the restriction in current implementations of kinematic simulation to Eulerian flow fields having a Gaussian structure. As we show in § 3 below, many of the striking scaling properties of velocity increments in turbulent flows can be reproduced by fields parameterized by only the first four moments. Details of the parameterizations are given in the Appendix.

3. Eulerian modelling

3.1. *Probability density function transport equation*

For a given two-point separation and corresponding velocity increment in space, an exact p.d.f. transport equation can be derived which relates the velocity spatial increment p.d.f. to the conditional accelerations (Borgas & Yeung 1998; Pope 2000). For the quasi-one-dimensional separation distance (Kurbanmuradov 1997) we have

$$\frac{u}{l^2}\frac{\partial l^2 P_E}{\partial l} = -\frac{\partial a P_E}{\partial u}, \tag{13}$$

where $P_E(u;l)$ is the p.d.f. of separation speed u for given separation l, and $a(u;l) \equiv \langle \dot{u}|u, l\rangle$ is the conditional rate of change (in time) of the separation speed.

Equation (13) provides a one-to-one correspondence between a and P_E, thus avoiding the non-uniqueness difficulty arising in three-dimensional models. However, because the conditional acceleration $a(u;l)$ is unknown, this equation is still unclosed. Borgas & Yeung (1998) proposed a quadratic-form closure in terms of the first four moments of the velocity increment, in the form

$$a = \alpha + \beta u + \gamma u^2, \tag{14}$$

where the coefficients $\alpha = \alpha(l)$, $\beta = \beta(l)$ and $\gamma = \gamma(l)$ are functions of the separation. For reasons explained later (see § 3.2), the distribution of u is truncated beyond the finite bounds u_+ and u_- which are to be specified. While (14) is a very good and simple-to-use approximation of DNS data (Borgas & Yeung 1998), its functional form does not always guarantee a realizable solution for the Eulerian p.d.f. in (13). To achieve realizability we propose a more general form

$$a = \alpha + \beta u + \gamma u^2 + b(u, l) \qquad (u_- \leqslant u \leqslant u_+), \tag{15}$$

where the additional function $b(u, l)$ is to be determined, although empirical evidence is that it is 'small' compared to the leading-order quadratic-form nature. This is our 'prior' assumption which guides our construction of a realizable, approximately quadratic form, drift term. The formulation is coupled with a quasi-similarity form $P_E(u;l) = \sigma^{-1} f(\vartheta;l)$, where $\vartheta = u/\sigma$, and $\sigma^2 = \langle u^2\rangle$. Substitution of (15) into (13) leads to the following equation for $f(\vartheta;l)$:

$$\frac{2\vartheta}{l} f + \vartheta\frac{\partial f}{\partial l} - \vartheta\frac{\sigma'}{\sigma} f - \vartheta^2\frac{\sigma'}{\sigma}\frac{\partial f}{\partial \vartheta} = -\frac{1}{\sigma^2}\frac{\partial(\alpha + \beta\sigma\vartheta + \gamma\sigma^2\vartheta^2 + b) f}{\partial \vartheta}, \tag{16}$$

where σ' is defined to be $\mathrm{d}\sigma/\mathrm{d}l$. It is useful to partition (16) into two equations, as:

$$\frac{2\vartheta}{l}f - \vartheta\frac{\sigma'}{\sigma}f - \vartheta^2\frac{\sigma'}{\sigma}\frac{\partial f}{\partial\vartheta} = -\frac{1}{\sigma^2}\frac{\partial(\alpha+\beta\sigma\vartheta+\gamma\sigma^2\vartheta^2)f}{\partial\vartheta}, \tag{17}$$

$$\vartheta\frac{\partial f}{\partial l} = -\frac{1}{\sigma^2}\frac{\partial bf}{\partial\vartheta}. \tag{18}$$

which we check, after solution, is consistent with sufficiently small b. This partition allows for explicit solutions, in part because (17) is effectively just an ordinary differential equation in ϑ. If f were strictly self-similar it would be entirely independent of l, in which case (18) would become

$$\frac{\partial bf}{\partial\vartheta} = 0, \tag{19}$$

so that the correction term $b(u;l)$ vanishes. This property is precisely why the particular partition of (16) was chosen. Conversely, this implies that non-zero $b(u;l)$ only occurs with deviations from strict self-similarity, or equivalently to the transition of the p.d.f. between different scaling ranges: from dissipation range to inertial range, then from inertial range to large scales. Because such scaling transitions are not abrupt, b is controllably small and this is demonstrated by example below.

The quadratic-form closure within (17) can now be determined in terms of the first four Eulerian moments of the velocity increments, which are written as

$$\langle u\rangle = 0, \quad \sigma^2 = \langle u^2\rangle, \quad \kappa = \langle u^3\rangle, \quad \varpi = \langle u^4\rangle. \tag{20}$$

Solutions for the coefficients in the case of unbounded velocity ($|u_\pm|\to\infty$) are

$$\tilde\alpha = (2\lambda+1)+1-\tilde\gamma, \tag{21a}$$

$$\tilde\beta = \tfrac{1}{2}(2\lambda+1)S + (1-\tilde\gamma)S, \tag{21b}$$

$$\tilde\gamma = 1+\tfrac{1}{3}(2\lambda+1)\frac{F-3-\frac{3}{2}S^2}{F-1-S^2}, \tag{21c}$$

where the parameters $\alpha=\sigma\sigma'\tilde\alpha$, $\beta=\sigma'\tilde\beta$, $\gamma=\tilde\gamma\sigma'/\sigma$, $\lambda^{-1}=l\sigma'/\sigma$, $S=\kappa/\sigma^3$ and $F=\varpi/\sigma^4$ are all functions of the separation l. Furthermore, (18) provides the correction to the drift term needed for realizability in Eulerian statistics. To see this, we note that for the given quadratic-form closure (21), (17) can be rearranged to

$$f^{-1}\frac{\partial f}{\partial\vartheta} = -\frac{\tilde\beta+(2\lambda+2\tilde\gamma-1)\vartheta}{\tilde\alpha+\tilde\beta\vartheta+(\tilde\gamma-1)\vartheta^2}. \tag{22}$$

This can be integrated by standard methods (Gradshteyn & Ryzhik 1980, p. 68) to give

$$f = \aleph(\tilde\alpha+\tilde\beta\vartheta+(\tilde\gamma-1)\vartheta^2)^{(\tilde\gamma+\lambda-\frac{1}{2})/(\tilde\gamma-1)}\exp\left[\frac{2\tilde\beta}{\Delta}\left(\frac{\lambda+\frac{1}{2}}{\tilde\gamma-1}\right)\arctan\left(\frac{\tilde\beta+2(\tilde\gamma-1)\vartheta}{\Delta}\right)\right], \tag{23}$$

where

$$\Delta = \sqrt{4\tilde\alpha(\tilde\gamma-1)-\tilde\beta^2}, \tag{24}$$

and the normalization factor $\aleph=\aleph(l)$ is determined by numerical integration so that

$$\int_{\vartheta_{min}}^{\vartheta_{max}} f(\vartheta')\,\mathrm{d}\vartheta' = 1. \tag{25}$$

A necessary condition for a real-valued solution is that $\tilde{\gamma} > 1$. From (21*c*), this condition corresponds to the inequality $F \geqslant 3 + 3S^2/2$, which is usually well satisfied in dispersion applications. (Note that, as proved in Kendall & Stuart (1969, p. 92), $F \geqslant S^2 + 1$ for any random process.) In addition, by inserting (21) into (24), a sufficient condition for real solutions is that $F \geqslant 3 + 15S^2/8 + O(S^4)$, which again is not a significant restriction in practice provided that the Eulerian skewness $|S|$ is small enough. Indeed, generally $|S| \leqslant 1/2$ so that dissipation range flatness greater than 3.5 is sufficient for real solutions.

Finally, when the realizability correction term, b, is prescribed by the integration in (18):

$$b = f^{-1}\sigma^2 \int_{\vartheta}^{\infty} \vartheta' \frac{\partial f}{\partial l}\, \mathrm{d}\vartheta', \tag{26}$$

substitution of (22) into (26) gives the realizability correction term (which remains non-trivial) as

$$\sigma^{-2} b = \frac{\tilde{\alpha}' + \tilde{\beta}'\vartheta + \tilde{\gamma}'\vartheta^2}{2\lambda + 1} - 2\frac{\tilde{\alpha} + \tilde{\beta}\vartheta + (\tilde{\gamma} - 1)\vartheta^2}{(2\lambda + 1)^2}\lambda' + \frac{\tilde{\alpha} + \tilde{\beta}\vartheta + (\tilde{\gamma} - 1)\vartheta^2}{2\lambda + 1}\frac{1}{f}\frac{\partial f}{\partial l}. \tag{27}$$

With these constructions, it follows that (23) is also a solution of the full transport equation, (16), which is the sum of (17) and (18) and is equivalent to (13). This gives a realizable solution for the Eulerian p.d.f., expressed conveniently for both the Eulerian velocity distribution and the conditional Eulerian acceleration. Moreover, the solution is, by design, close to having quadratic-form conditional accelerations as in (15). This solution is shown below (§ 3.3) to give a good representation of DNS Eulerian properties.

3.2. *Probability density function tails and finite velocity range corrections*

A key property of the form (23) for the Eulerian velocity increment p.d.f. is that, at large ϑ, the exponential factor becomes a constant (with $\arctan(\pm\infty) = \pm\pi/2$). This implies the modelled p.d.f. has power-law tails in ϑ, of the form:

$$P_E \sim |\vartheta|^{-2(\tilde{\gamma} + \lambda - 1/3)/(\tilde{\gamma} - 1)}. \tag{28}$$

This power-law behaviour is in contrast to the one-point velocity p.d.f., which for isotropic turbulence is close to Gaussian (Jimenez 1998). Gaussianity of the velocity component, say $u_1^{(1)}$, of a single fluid particle implies that the probability of occurrence of large $u_1^{(1)}$ decreases in the limit exponentially fast in the square of the velocity. A similar decrease in the tails is expected also for the joint p.d.f. of the velocities of two fluid particles. Consequently, the power law form in (28) overestimates the probability of occurrence of very large values of ϑ, which corresponds to at least one fluid particle velocity component approaching infinite values. To prevent this latter pathological situation in the model, the power law is truncated at some finite range, by setting $P_E(u;l) = 0$ for both $\vartheta > \vartheta_{max}$ and $\vartheta < \vartheta_{min}$. In reality, of course, p.d.f. tails close to Gaussian or to stretched exponential forms (Frisch 1995; Sornette 2000) are quite common models. However, our assumption here is that truncated power-law behaviour captures the critical physics and that the precise form of the far tails of the p.d.f. is not essential.

For velocities restricted to a finite range, the expressions in (21) can be formally modified to include several correction terms, as:

$$\left.\begin{aligned}\tilde{\alpha} &= (2\lambda+1)+1-\tilde{\gamma}+\Delta_1,\\ \tilde{\beta} &= \tfrac{1}{2}(2\lambda+1)+S(1-\tilde{\gamma})+\tfrac{1}{2}\Delta_2,\\ \tilde{\gamma} &= 1+\tfrac{1}{3}\frac{\Delta_3-\frac{3}{2}S\Delta_2-3\Delta_1}{F-1-S^2}+\tfrac{1}{3}(2\lambda+1)\frac{F-3-\frac{3}{2}S^2}{F-1-S^2},\end{aligned}\right\} \tag{29}$$

where

$$\Delta_m = [\vartheta^m(\alpha+\beta\vartheta+\gamma\vartheta^2)f]_{\vartheta_{min}}^{\vartheta_{max}} \tag{30}$$

for each of $m=1, 2, 3$, and ϑ_{min} is obtained for chosen ϑ_{max} by the nonlinear equation

$$[(\alpha+\beta\vartheta+\gamma\vartheta^2)f]_{\vartheta_{min}}^{\vartheta_{max}} = 0. \tag{31}$$

In principle, ϑ_{max} can be treated as a parameter to be specified based on knowledge of Eulerian statistics, or used as a free parameter to tune the model results for best agreement with DNS or experiments. However, in our calculations, provided the magnitudes of ϑ_{max} and ϑ_{min} are large enough, the correction factors Δ_1 and Δ_2 are generally small. The main exception (based on calculations reported below) is the case when the Eulerian flatness factor exceeds about seven. This is expected to occur only for the very smallest separations, at the largest Reynolds numbers, and is only relevant for short times in Lagrangian evolutions. In other words, in most situations, the finite-range correction terms are small and can be neglected. Indeed we use the simpler explicit approximation (21) for the rest of the paper, with the caveat that neglect of finite-range correction terms may be a factor in the under-prediction of flatness factors in the Lagrangian results at early times for small initial separations.

3.3. *Eulerian results and comparison with DNS*

Here, we present some sample results for the Eulerian quantities described in the two preceding subsections. Figure 1 shows modelled Eulerian velocity p.d.f.s at Taylor-scale Reynolds number (R_λ) approximately 230, averaged in time over the length of a 512^3 simulation in DNS (Part 1). The separation distance l is varied from the dissipation to energy-containing ranges: the smallest l corresponds to one grid spacing, whereas the largest value is half of the length of the solution domain (and about three times the integral length scale of the turbulence). The data are shown for $\vartheta = u/\sigma$ between $+5.5$ and -5.5, corresponding roughly to ϑ_{min} and ϑ_{max} used in the rest of the paper. It can be seen that the modelled p.d.f.s agree well with non-Gaussian and negative skewness properties for small separation, but are trending to Gaussian for large separations. The scale size (l) which is closest to inertial range is the case $l/\eta = 98$, for which the p.d.f. is seen to be mildly non-Gaussian, with a slight but significant negative skewness.

Corresponding results for conditional acceleration are shown in figure 2. The results here are close to the simple quadratic form proposed in Borgas & Yeung (1998, figure 6 therein) without the realizability correction term $b(u;l)$ as introduced in this paper. Thus, the results also represent reasonably well the appropriate DNS data reported in Borgas & Yeung (1998, figure 5 therein). However, it is interesting to note that, for large separations, the realizability correction gives a flatter profile for the conditional acceleration at large negative u, but a steeper profile at large positive u. The DNS data show rapid fall-off at the extreme tails, perhaps affected by sampling error. This discrepancy in the tails at large separation suggests that a separation-dependent

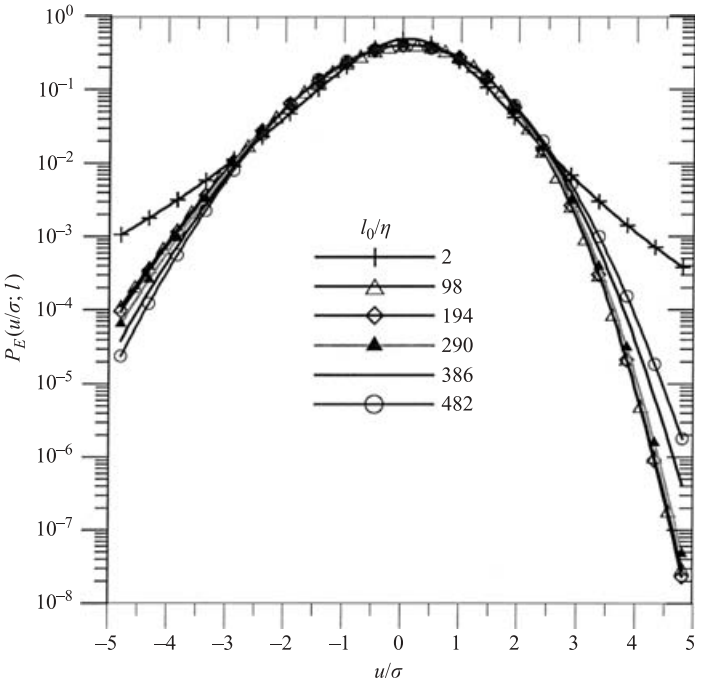

FIGURE 1. Eulerian p.d.f.s for the longitudinal velocity increment as a function of separation, at $R_\lambda = 230$; generated from the modelled transport equation (16).

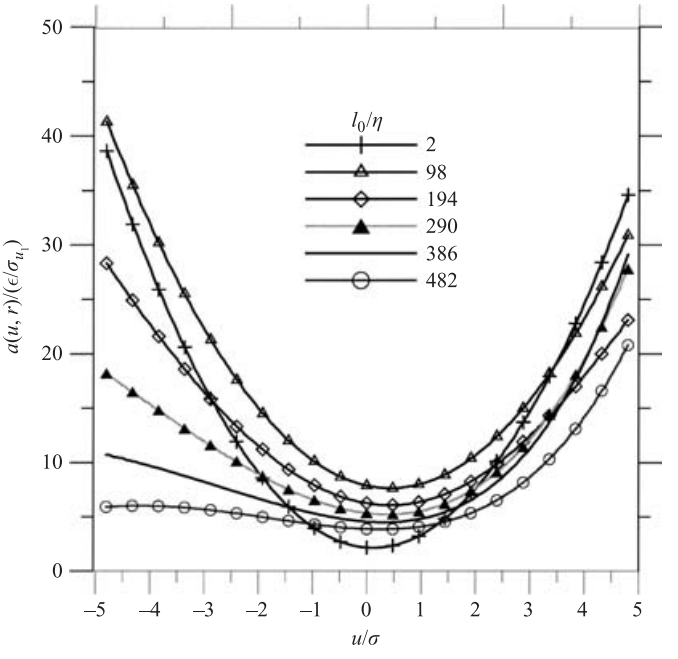

FIGURE 2. Eulerian conditional accelerations given the longitudinal velocity increment, corresponding to the p.d.f. results in figure 1.

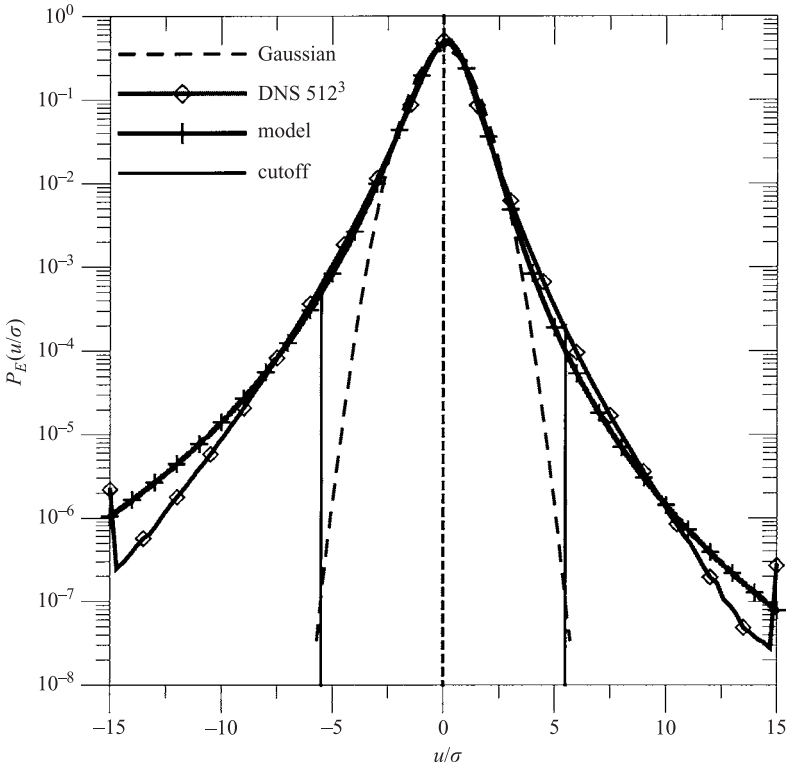

FIGURE 3. Eulerian p.d.f.s for the longitudinal velocity increment at a fixed separation of $l_0/\eta = 2$ corresponding to DNS data at $R_\lambda = 230$ on a 512^3 grid. DNS data (open diamonds) are compared with model (crosses) and with a Gaussian p.d.f. (dashed line). The approximations for faster than power-law cutoff are shown with solid vertical lines. The DNS tails beyond $u/\sigma = \pm 15$ are lumped into the last bin.

truncation, with say $\vartheta_{max}(r) \to \infty$ as $r/\eta \to \infty$, may be needed to capture the large-scale Gaussian limit more accurately.

Figure 3 shows a direct comparison between model and DNS, for the velocity p.d.f. at $R_\lambda = 230$ and $l/\eta = 2$. At this small separation within the dissipation range, where non-Gaussian effects are strongest, the two-point velocity difference is nearly proportional to the velocity gradient, which has intermittent behaviour exhibited in a wide tail. The model is seen to reproduce DNS results closely within ± 5 standard deviations. However, it is also clear that the power-law tail of the model overestimates the likelihood of large-amplitude separation velocities. For reasons explained in § 3.2, we truncate the model p.d.f. at $\{\vartheta_{min}, \vartheta_{max}\} = \{-5.5, 5.5\}$, respectively.

The sensitivity of the truncation for Eulerian properties is mild, so that we are free to choose widely even up to the point of no finite truncation. However, the Lagrangian properties are sensitive to the truncation and some Lagrangian trajectories cluster around large separation velocities, up to the point that very rapid sustained separation is possible. The flexibility of robust Eulerian properties, insensitive to the specific bounding separation velocity, allows effective control of the rapid acceleration process for Lagrangian trajectories and permits the genesis of the highly non-Gaussian behaviour we are trying to model. In the same context, an inappropriate Eulerian p.d.f., say with Gaussian-like tails for large velocities (and exponentially small frequencies),

will over-control the rapid separation process and prevent the genesis of highly non-Gaussian behaviour. In fact, this is precisely the case evident from previous stochastic models.

In summary, the Eulerian properties are efficiently parameterized by the current corrected-quadratic-form model. The p.d.f. of Eulerian separation velocities and the conditional-mean-acceleration are derived as simple functions of the conditioning velocity and separation scale, with prescribed variance, skewness and flatness. The form of these solutions agrees well with the DNS Eulerian statistics, and the simple functional forms facilitate the development of stochastic models to address the problem of predicting Lagrangian statistics, which is the main object of relative dispersion study.

3.4. *Flow structure: straining and streaming regions*

In view of recent interest in the kinematic simulation approach (Malik & Vassilicos 1999), a brief discussion is useful on how spatial structural elements in KS are represented by Lagrangian stochastic models. The three major structural patterns recognized in KS are: straining regions, where instantaneous streamlines converge in one direction and diverge in another; streaming regions, where streamlines are nearly parallel; and finally eddying regions, where recirculating streamlines indicate local rotation of fluid elements. In our model, straining regions are characterized by large positive values for u corresponding to diverging streamlines where particle pairs separate, while negative values of u indicate converging streamlines where particles approach each other. Because of incompressibility, converging and diverging streamlines generally form a pair (at a hyperbolic point) and thus occur with similar frequency (this explains the similar 'flaring' of the p.d.f. at either large positive or negative strain rates). Streaming regions where particle pairs mainly move together are represented by values of $|u|$ of small magnitude, whereas the highly-rotational and eddying regions are represented by rapid changes in the direction of the separation vector, rather than in the magnitude, so again $|u|$ is small. The dominant dynamical process for relative dispersion is clearly high-u straining. Together with the ergodic hypothesis for turbulent flow, our detailed description of the Eulerian velocity p.d.f. ensures that the spatial distribution of 'straining' and 'streaming' regions is faithfully represented. The use of Eulerian velocity structure functions as model input also allows for non-Gaussianity of the small scales, and is an improvement over a Gaussian flow field, where the occurrence of flow regions with high strain rate would be grossly under-represented.

4. Lagrangian modelling

4.1. *Diffusion in velocity phase space*

Quasi-one-dimensional models of dispersion based on a Langevin-type equation for the velocity (7) can be written in the form

$$\begin{aligned} \mathrm{d}u &= A(u,l)\,\mathrm{d}t + \mu(l)\,\mathrm{d}W, \\ \mathrm{d}l &= u\,\mathrm{d}t, \end{aligned} \tag{32}$$

where $A(u,l)$ is a drift term, and μ is a scale-dependent diffusion coefficient. In terms of the Thomson (1987) stochastic model approach, the drift term is constrained by the Eulerian flow statistics and, in fact, is closely related to the conditional accelerations (15). The Markov stochastic model formulation is best approximated at high Reynolds number and for time increments substantially larger than the Kolmogorov time scale ($\tau_\eta = \sqrt{\nu/\overline{\epsilon}}$), and spatial increments somewhat larger than η. In this paper, we attempt

to adapt the model to describe diffusion in velocity phase space with explicit relaxation processes due to viscous forces as parameterized by the scale-dependent stochastic noise amplitude $\mu(l)$. This adaptation is contrived, but is sufficiently flexible and constrained to lead to useful model development as demonstrated by results obtained below.

In the limit of particles far apart, and which move almost independently of each other, the scale dependence of $\mu(l)$ is expected to be relatively weak. It is thus reasonable to let $\mu(l)$ approach a constant, i.e.

$$\mu = \mu(l) \to \mu_\infty \quad \text{as} \quad l/\eta \to \infty. \tag{33}$$

Classical inertial-range reasoning for Lagrangian velocity structure functions (see Sawford 2001) gives

$$\langle (v(t+\tau) - v(t))^2 \rangle \sim C_0 \overline{\epsilon} \tau, \tag{34}$$

where v is one component of a single fluid-particle velocity and C_0 is a constant. This then implies that $\mu_\infty = (2C_0\overline{\epsilon})^{1/2}$, at least in the high-Reynolds-number limit. This is because for very small time increments, the change of separation velocity (when l is large) is dominated by the difference between two independent single particle motions. The constant C_0 is important in Lagrangian turbulence theory and plays an equivalent role to the Kolmogorov inertial range constant in the Eulerian second-order structure function. Recent estimates (Sawford & Yeung 2001; Yeung 2002) put C_0 in the range between 6 and 7. However, at the moderate Reynolds numbers typical in DNS, we shall let the corresponding model coefficient (denoted by $\tilde{C}_0$) vary with Reynolds number, with C_0 itself taken as the asymptotic value.

In the limit of small separation, viscous effects smooth out sharp spatial gradients and make the two-point difference in acceleration vanishingly small. This suggests that a series expansion of the type $\mu = \mu_1 l + \mu_2 l^2 + \ldots$ (where μ_1, μ_2 are new model parameters) may be applicable. In addition, we may expect that for larger values of l/η, viscous effects would fall off exponentially fast. We use an expression which satisfies these expectations, as

$$\mu = (2\tilde{C}_0\overline{\epsilon})^{1/2}\{1 - \exp[-(\mu_1 l/\eta\sqrt{2\tilde{C}_0})^m]\}^{1/m}, \tag{35}$$

where m is an interpolation parameter that governs how quickly the transition between dissipation range and large-scale behaviour occurs with increasing l/η.

4.2. *The drift term*

Given the stochastic forcing, the drift term in (32) can be determined with Thomson's well-mixed argument (Thomson 1990; Kurbanmuradov 1997): the stochastic model (32) corresponds to the Fokker–Planck equation (Gardiner 1985, p. 96) with drift term $A(u, l)$

$$\frac{\partial P}{\partial t} + u\frac{\partial P}{\partial l} = -\frac{\partial AP}{\partial u} + \tfrac{1}{2}\mu^2\frac{\partial^2 P}{\partial u^2} \tag{36}$$

for the transition p.d.f. $P(u, l, t; u_0, l_0, t_0)$, of separation distance l and its time derivative, u. The Eulerian counterpart of this equation (Thomson 1990; Kurbanmuradov 1997; Borgas & Yeung 1998) is a modelled transport equation of the form

$$\frac{u}{l^2}\frac{\partial l^2 P_E}{\partial l} = -\frac{\partial AP_E}{\partial u} + \tfrac{1}{2}\mu^2\frac{\partial^2 P_E}{\partial u^2} \tag{37}$$

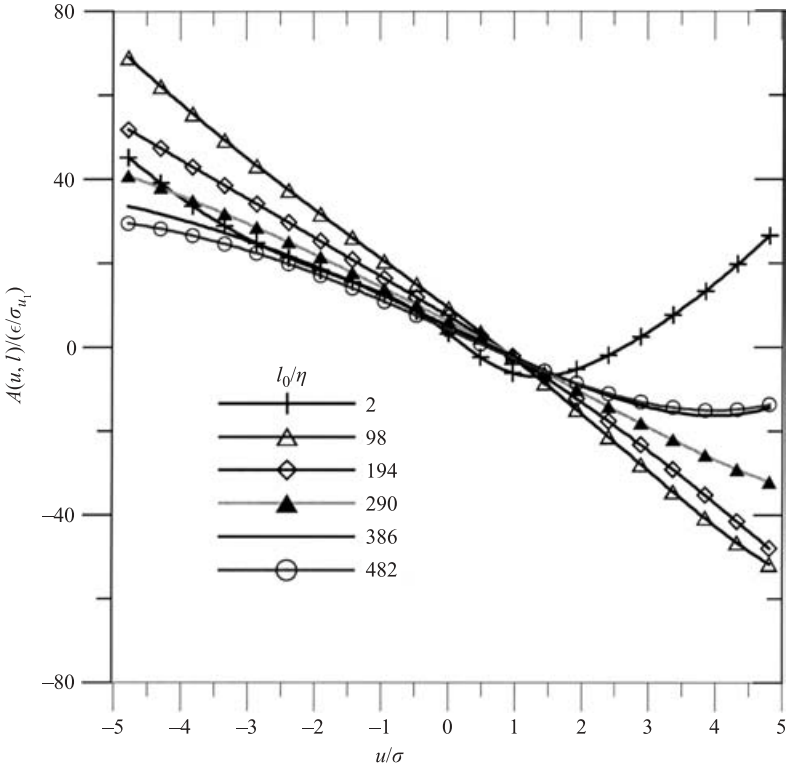

FIGURE 4. Drift term for the stochastic equation as a function of longitudinal velocity increment and for various fixed separations, at $R_\lambda = 230$. The large separation limit approaches the linear drift term for particles moving independently.

for the Eulerian velocity p.d.f., $P_E(u;l)$. Comparison of this with the exact p.d.f. transport equation (13), leads to the constraint

$$\frac{\partial(A-a)P_E}{\partial u} = \tfrac{1}{2}\mu^2\frac{\partial^2 P_E}{\partial u^2}, \tag{38}$$

which may be integrated with respect to u to give the relationship

$$A(u,l) = a(u,l) + \tfrac{1}{2}\mu^2\frac{\partial \ln P_E}{\partial u}. \tag{39}$$

Using the Eulerian parameterization derived for P_E (based on (23) for f), we obtain

$$A(u,l) = a(u,l) - \tfrac{1}{2}\mu^2\frac{\beta + 2\big(\gamma - \tfrac{1}{2}\sigma'/\sigma + 1/l\big)u}{\alpha + \beta u + (\gamma - \sigma'/\sigma)u^2}. \tag{40}$$

In other words, the drift term can be explicitly related to the conditional acceleration $a(u,l)$ which is in turn evaluated using the quadratic closure in § 3.1 together with the realizability correction $b(u,l)$. The drift term calculation allowed by these expressions is quite efficient. This is useful for numerical implementation because, to capture the highly non-Gaussian features that we examine, it is necessary to compute a large number of samples with independent stochastic-model realizations.

Drift terms computed according to the models above are shown in figure 4, for the same Reynolds numbers and spatial separations as for the conditional acceleration shown in figure 2. Choices for additional model parameters are $\mu_1 = 0.7$, $m = 1.8$

and $\tilde{C}_0 = 9$. This high value of $\tilde{C}_0$ (higher than the asymptotic limit $C_0 \sim 6 - 7$) is a consequence of the collective choice of all interpolation parameters in (35). We have chosen here to focus on the small-scale properties of the relative dispersion process at finite Reynolds number. Thus, because the value of $\tilde{C}_0$ primarily affects large-time results by altering the modelled Lagrangian integral time scale, and it does not have much impact on statistics in the dissipation range, there is no need to better parameterize large-scale properties. In figure 4 we can see that, overall, the drift term deviates substantially in shape from the quadratic-form conditional acceleration and is far more skewed. This distortion in form is also markedly non-monotonic in respect of scale size l/η, being most pronounced for $l/\eta = 98$, which is nominally in the inertial subrange. In the limit of large separation, the model is, in principle, compatible with an unbounded Gaussian velocity p.d.f. as the motions of particles far apart become independent. Nevertheless, because we truncate the p.d.f. to a fixed finite range (§ 3.2), significant deviations are still expected, and are indeed seen in the $A(u, l)$ curve, with undulations about the asymptotic straight line with negative slope.

5. Numerical implementation

Numerical methods in our modelling are relatively straightforward. First, the initial separation is assigned and, for each realization, an independent initial random separation speed is drawn from the appropriate Eulerian probability distribution. Each trajectory is integrated in time using adaptive time-stepping, which helps ensure numerical stability. Restriction of separation speed to a finite range also helps ensure that the model is stable and free of singular behaviour due to large separation speeds.

The initial particle-pair separation speeds are chosen randomly according to the Eulerian p.d.f. parameterized in (23). We use a standard procedure for drawing random variables based on the cumulative distribution function. For a given separation distance l we define

$$F(u_r; l) = \int_{-\infty}^{u_r} f(v; l)\, \mathrm{d}v, \tag{41}$$

which is bounded between 0 and 1. A sample of a random variable, say χ, uniformly distributed between 0 and 1 is first drawn by calling a random number generator routine. The corresponding value of the initial velocity (u_0) is then obtained by solving $F(u; l) = \chi$. This last step can be carried out easily by interpolation based on tabulated function values of $F(u; l)$ for l equal to the initial separation l_0.

The discretized form of the equation system (32) can be written as

$$\left.\begin{aligned} u_{n+1} &= u_n + A(u_n, l_n)\Delta t + \mu_n \sqrt{\Delta t}\,\xi_n, \\ l_{n+1} &= l_n + u_n \Delta t. \end{aligned}\right\} \tag{42}$$

where Δt is the time increment between t_n and t_{n+1}, and ξ_n is a Gaussian random variable of zero mean and unit variance. A simple 'reflective' condition is used to restrict the velocity to a finite range: e.g. if u_{n+1} from (42) falls outside the range (u_{min}, u_{max}) it is just recalculated with a sign change in either or both the drift term and the random term (first the drift term, then the random term, then the two together stopping when u_{n+1} is in range).

The size of time step Δt must be chosen carefully. It is clear that, in order to resolve the small-scale dynamics, Δt should be much smaller than the Kolmogorov time scale τ_η. Strong intermittency at early times and for small initial separation also makes this requirement more demanding. On the other hand, at later times, as separation

statistics evolve on much longer time scales, a larger Δt can be used (which helps reduce CPU costs). Consequently, we use an adaptive scheme which gives a small Δt at earlier times, but larger Δt at later times or when the separation distance for a given particle pair has become large. Specifically, we have

$$\Delta t = \begin{cases} 0.01\tau_\eta & t_n \leqslant 20\tau_\eta, \\ 0.01\tau_l & t_n \geqslant 20\tau_\eta, \end{cases} \tag{43}$$

where $\tau_l \equiv \sigma^2(l)/\overline{\epsilon}$ is a turbulence time scale associated with the instantaneous separation distance l. This time-stepping strategy recognizes that (at least for the smallest initial separations in this paper, $l_0/\eta = 1/4$) the critical non-Gaussian dynamics occurs within the first 20 Kolmogorov time scales. The numerical factor of 0.01 times the relevant evolution time scale is typical for stochastic models, and tests have shown that it is adequate in our work. We also allow Δt to be adjusted suitably in order to produce output statistics at regularly spaced time intervals.

The use of very small Δt at early times, as noted above, is closely related to the need to avoid the occurrence of singularities in the model implementation. Simple stochastic equations with quadratic drift terms are known to give rise to singular behaviour with infinite solutions in finite time (Gardiner 1985), which in our case can give infinitely large Lagrangian velocities if a modelled Eulerian p.d.f. with unbounded velocity were adopted. If a singularity begins to form, extremely small time steps must be used to resolve the situation numerically; overall this tends to make the modelling more difficult. However, as discussed in § 3.2, we are able to avoid this difficulty by imposing finite bounds on the velocity. We emphasize that this does not affect the ability of the model to reproduce non-Gaussian aspects of relative dispersion.

To obtain reliable statistical results from the simulated trajectories, the number of independent particle-pair samples (N) must be sufficiently large. The estimation of model statistical sampling errors, with respect to sample size N, is similar to that for a large number of particles and particle-pairs in DNS (Part 1, § 2.3). Stochastic model calculations with N as large as 10^6 (used for the estimation of the separation-distance p.d.f.s) are possible on desktop personal computers without the need for any high-performance computer platforms.

6. Model results and comparisons

In this section, we evaluate the performance of our new stochastic model, primarily by comparison with DNS for moments of the separation distance and the separation speed. We also discuss the shape of the separation distance p.d.f., in the light of classical Richardson scaling and some recent results from experiments. The DNS data are those in the companion paper (Part 1) on stationary isotropic turbulence at three Reynolds numbers, R_λ 90, 140 and 230 simulated on grids from 128^3 to 512^3. Initial separations range from 1/4 of a Kolmogorov length scale to longer than one integral length scale. The most demanding quantities for the model predictions are generally higher-order moments at relatively early times when intermittency is strong, and especially for small initial separations. The chosen parameters from (35), μ_1, m and $\tilde{C}_0$, are given in table 1. The values of these parameters are obtained by tuning the results for optimal agreement with DNS. All of the model parameters shown in table 1 show a strong and monotonic dependence on the Reynolds number. We show results explicitly for R_λ-90 and 230, but include R_λ-140 as an intermediate case in plots that illustrate Reynolds number trends.

Grid	128^3	256^3	512^3
R_λ	89	141	230
$\mu_1\eta/\sqrt{\bar{\epsilon}}$	0.5	0.53	0.69
m	1.0	1.25	1.75
$\tilde{C}_0$	7.0	7.5	9.0
u_{max}/u_{rms}	3.8	4.3	4.8

TABLE 1. Lagrangian model parameters.

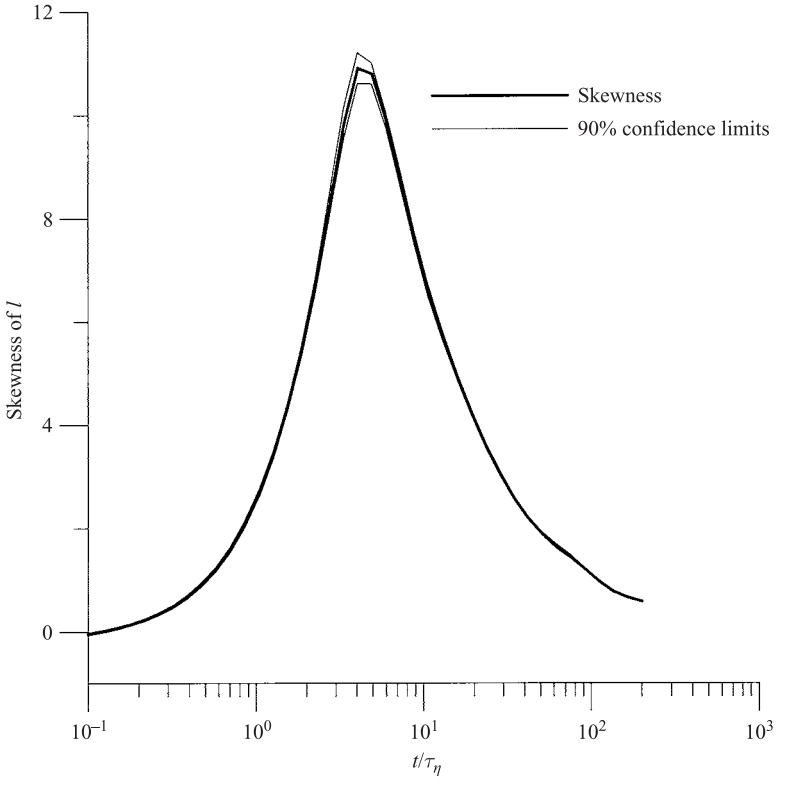

FIGURE 5. Statistical confidence limits for the evolution of skewness of the separation distance. These limits are computed using the Student's t test applied to 10 model ensembles of 10^5 realizations, for the $R_\lambda = 230$, $l_0/\eta = 1/4$ case.

For meaningful comparisons between DNS and stochastic modelling, it is clear that each must be implemented with sufficient sample size to ensure reliable statistics. In Part 1 statistical uncertainty in DNS was quantified via confidence intervals estimated by dividing the data into several subensembles. In figure 5, we show the results of a similar analysis, for the skewness of the separation distance at $R_\lambda = 230$ with initial separation $l_0/\eta = 1/4$. A Student's t-test is used to evaluate 90% confidence intervals, which are seen to be quite small. As suggested by this figure (and figure 1 of Part 1), the sampling variability in the stochastic model is substantially smaller than that observed from the DNS. The reason for this is that the stochastic model is for an ideal stationary system with statistics strictly independent of time, whereas in DNS, 'stationarity' is attained only in the sense of time averages taken over a relatively long

time interval. Indeed, in Part 1 we noted that during the $R_\lambda = 230$ simulation (where R_λ itself is a time average), the space-averaged energy dissipation varies in time by up to 80%, while instantaneous R_λ ranges from 190 to 250. In principle, sampling in DNS can be improved by making separate runs which are non-overlapping in time, but at present this is too expensive. Lesser statistical variability and better efficiency in allowing large numbers of realizations are favourable attributes of the model.

6.1. *Moments of separation distance*

The most important test of the model is whether the basic statistics of the separation distance are predicted well. In figure 6, we show information on the first four moments of the separation (as the mean, r.m.s, skewness and flatness) at $R_\lambda = 90$, compared directly with DNS. Clearly, except for some small differences at intermediate times, very good agreement is obtained. The mean and r.m.s are overall measures of how far apart the particle pairs become as time evolves, whereas skewness and flatness factors are quantitative measures of the shape of the probability distribution. The highly non-Gaussian nature of relative dispersion even at this modest Reynolds number has been noted before in the literature (Yeung 1994; Malik & Vassilicos 1999). It is especially encouraging to note that parameters in the present model can be tuned to reproduce this behaviour, which (in terms of large skewness and flatness factors) is most prominent at intermediate diffusion times for particle pairs of small initial separation. This success is a substantial improvement over most previous stochastic models (e.g. Heppe 1998) which were unable to capture higher-order statistics with sufficient accuracy. Effectively, we have shown that previous limitations discussed in the literature (Malik & Vassilicos 1999; Flohr & Vassilicos 2000) are not an inherent failure of stochastic models, but instead can be overcome by accounting for the behaviour of Eulerian velocity statistics in a careful manner (as in § 3), in particular accounting for fast separation speeds properly.

The large-time behaviour seen in figure 6 can be deduced analytically by making two assumptions. First, as the particles in each pair move far apart, their motions, and ultimately displacements, become mutually independent. In other words, the mean-square separation becomes twice the mean-square displacement of a single fluid particle which follows an asymptotic diffusive limit (Taylor 1921). We obtain

$$\langle l^2 \rangle = 3\langle l_1^2 \rangle \approx 12\sigma_u^2 T_L t \quad (t \gg T_L), \tag{44}$$

where T_L is the Lagrangian integral time scale based on the single-particle velocity autocorrelation. Secondly, as shown in Yeung (1994), the asymptotic form of the p.d.f. of l can be deduced by assuming that all coordinate components of the vector $\boldsymbol{l}$ become statistically independent and Gaussian. The first moment of this p.d.f. gives

$$\langle l \rangle \approx 4\sqrt{\frac{2}{\pi}}\sigma_u \sqrt{T_L t} \quad (t \gg T_L), \tag{45}$$

whereas the corresponding skewness and flatness factors are about 0.49 and 3.1 respectively. The model is seen to successfully reproduce these limits.

Similar comparisons are made in figure 7, at higher Reynolds number for $R_\lambda = 230$ corresponding to DNS results at the highest grid resolution given in Part 1. Stronger intermittency at this higher Reynolds number leads to greater uncertainties in the DNS data for skewness and flatness factors. With allowance for this limitation in DNS, it can be said that, overall (albeit again with some tuning of the model parameters), roughly the same level of agreement as in figure 6 is achieved. This suggests clearly that Reynolds-number trends are captured well by the model.

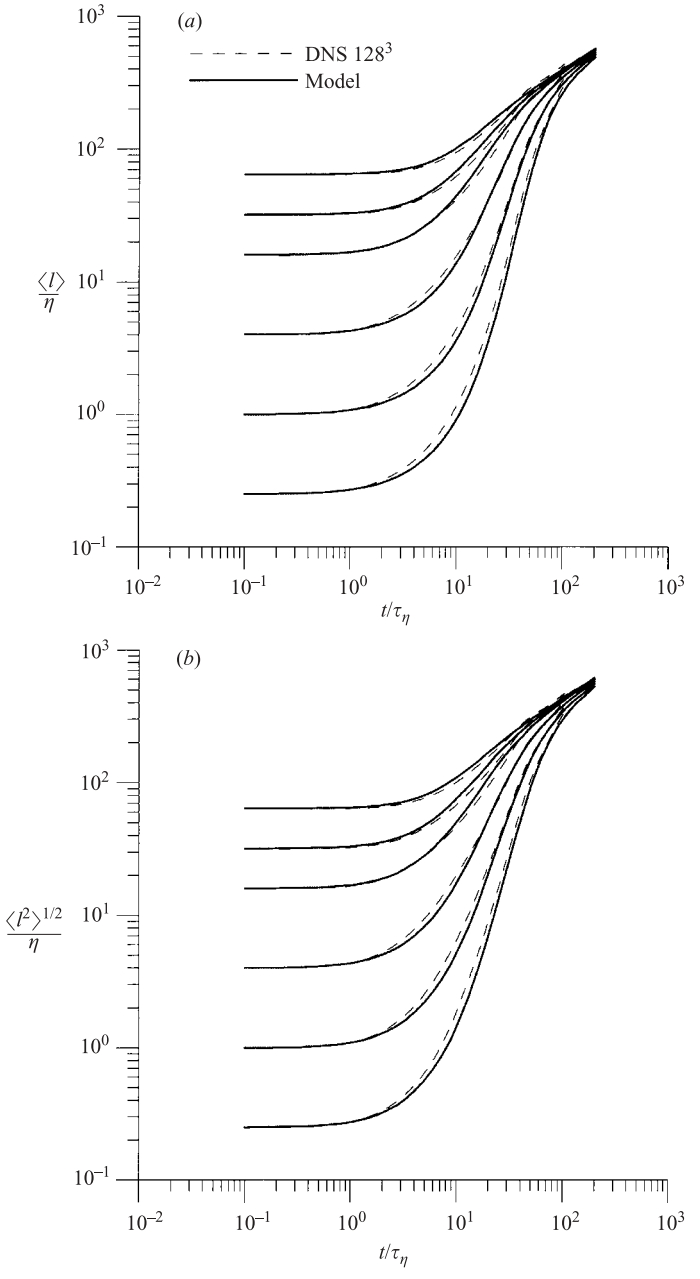

FIGURE 6(*a*, *b*). For caption see facing page.

It may be noted that at $R_\lambda = 230$, the initial flatness factor appropriate for the Eulerian flow field is quite large (over 7), and that the p.d.f. is stretched out relatively wide. As a result, at this higher R_λ, truncation of Eulerian velocity distribution to a finite range introduces greater errors. In turn, this leads to some systematic discrepancies at early times, where the fourth moment of the separation distance is under-predicted. The rapid loss of memory, however, leads to adequate Lagrangian modelling over most of the relevant time span.

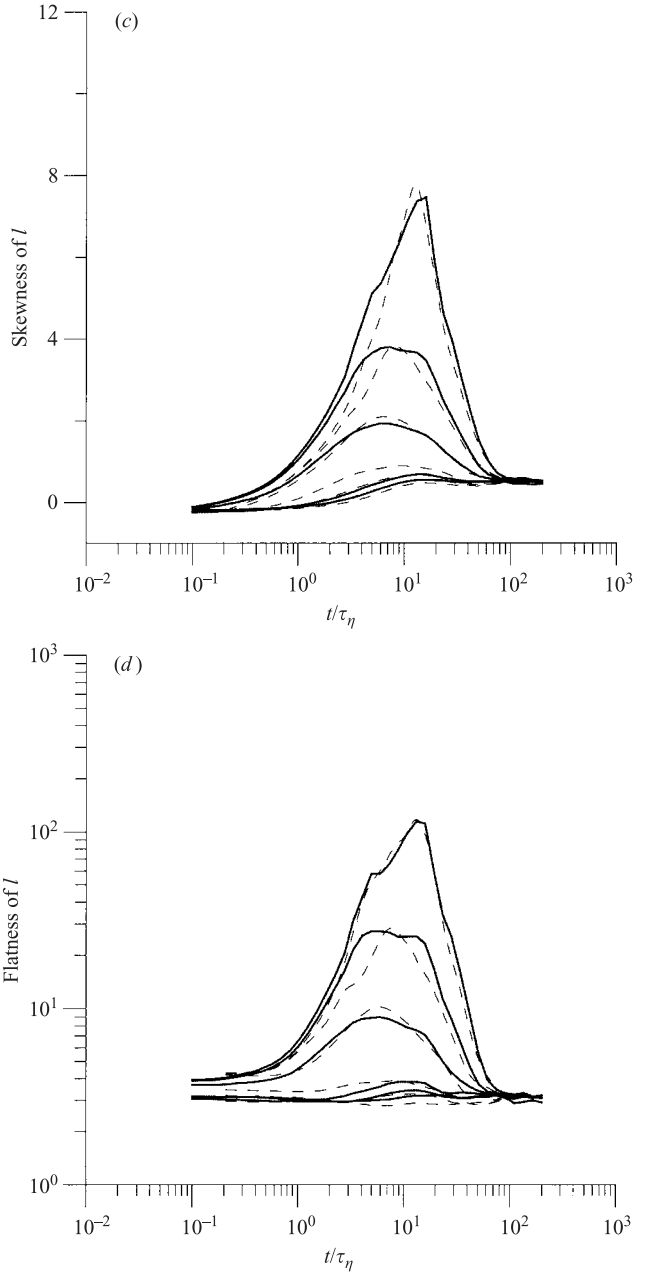

FIGURE 6. (*a*) Mean separation distance for various initial separations at $R_\lambda = 90$ (corresponding to 128^3 simulation); (*b*) root-mean-square separation distance; (*c*) skewness of the separation distance; and (*d*) flatness of the separation distance. In (*a*) and (*b*) the initial separation asymptote is evident at the left, and in (*c*) and (*d*) the curves generally increase with decreasing initial separation. Model and DNS (128^3) results are shown as solid lines and dashed lines, respectively.

To understand better the model representation of Reynolds-number dependence, we show in figure 8 data for three different Reynolds numbers, on the skewness and flatness of l with initial separation fixed at $l_0/\eta = 1/4$. These plots show that

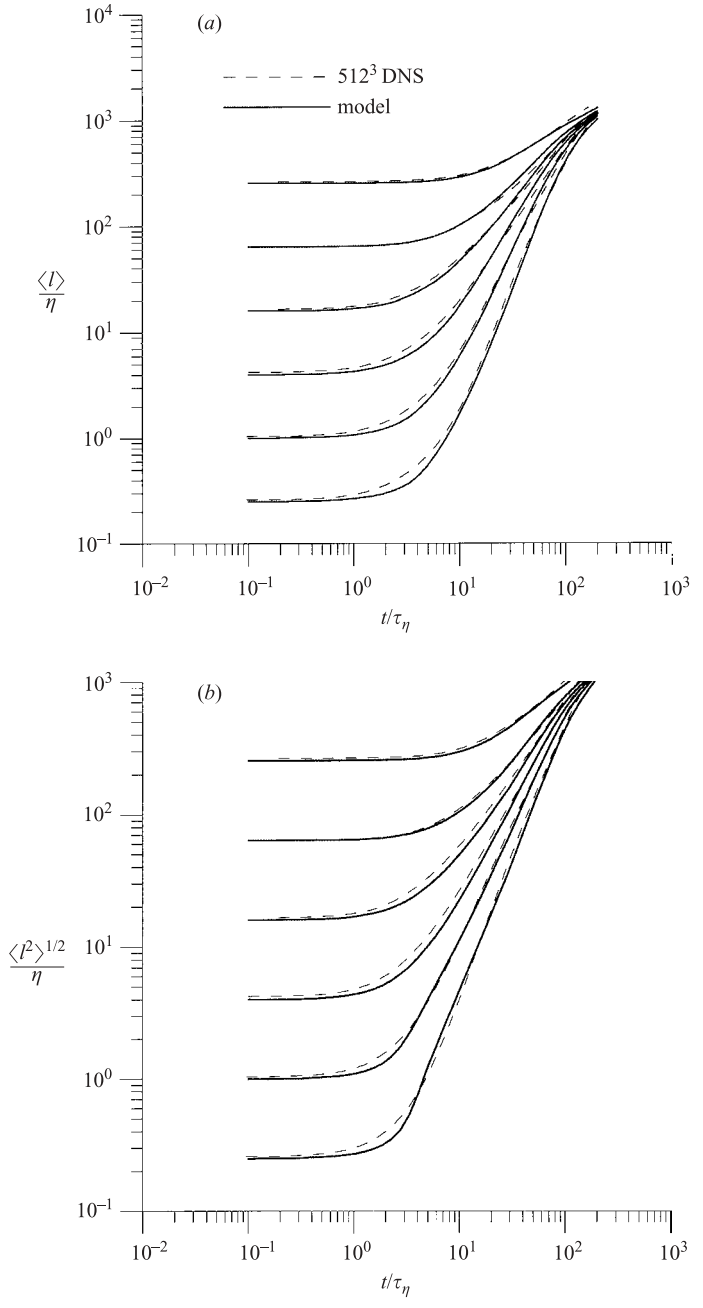

FIGURE 7(a, b). For caption see facing page.

as Reynolds number increases, the Lagrangian intermittency becomes stronger (with higher skewness and flatness). Furthermore, peak intermittency occurs earlier in time (even on a time scale normalized by τ_η). Both of these trends agree with those observed in DNS (Part 1).

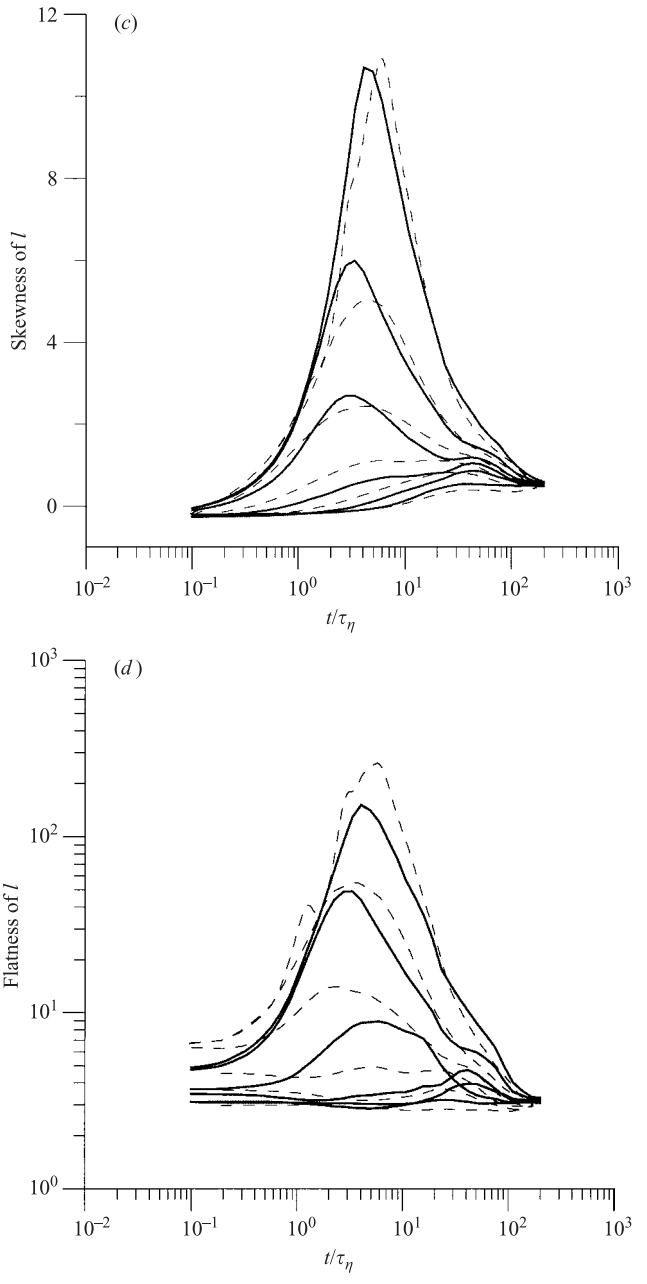

FIGURE 7. As for figure 6, but for $R_\lambda = 230$ corresponding to 512^3 DNS: (*a*) mean relative separation distance at $R_\lambda = 230$; (*b*) root-mean-square separation distance; (*c*) skewness of the separation distance; and (*d*) flatness of the separation distance.

6.2. *Moments of separation speed*

As a further check on model behaviour we now examine the statistics of the Lagrangian separation speed. The strategy of tuning the model parameters for optimal agreement for the statistics of separation distance leaves the separation speed statistics

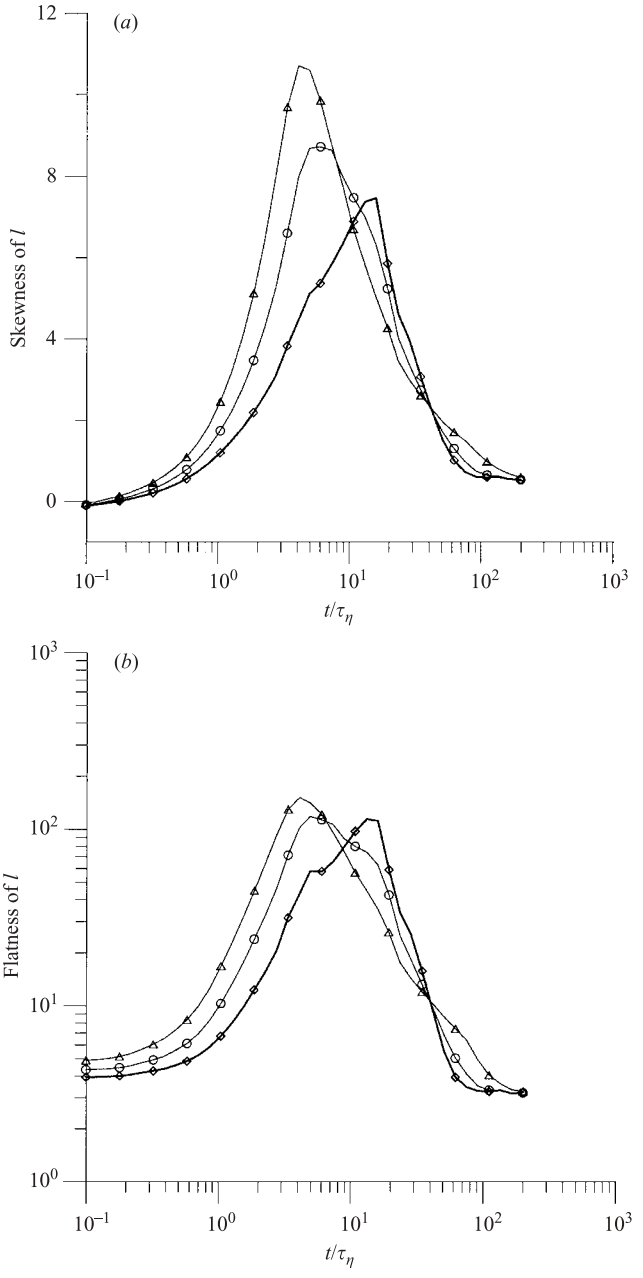

FIGURE 8. (*a*) Skewness of separation distance for three different Reynolds numbers ($\diamond$, $R_\lambda = 90$; $\circ$, 140; $\triangle$, 230) for fixed initial separations of $l/\eta = 1/4$. (*b*) Similar to (*a*), but for flatness of the separation distance.

as a stricter test of the model. Good agreement for the separation speed, especially in its higher-order moments, is indeed more difficult to achieve, in part because it is more intermittent than the separation distance.

In figure 9, we show comparisons with DNS at $R_\lambda = 230$ for the mean, r.m.s. and skewness and flatness factors of the separation speed, u. Because of the accelerating nature of the separation process, the mean separation speed is positive except at $t = 0$. Its value increases steadily with time until large-time behaviour gradually sets in (which occurs earlier for larger initial separations). Since $\langle u \rangle = \mathrm{d}\langle l \rangle / \mathrm{d}t$, it is clear that asymptotic $t^{1/2}$ behaviour in $\langle l \rangle$ (see (45)) implies a $t^{-1/2}$ decrease in $\langle u \rangle$. It can be seen that the model follows the DNS data trend quite well, except that the eventual large-time decrease appears to occur earlier than expected, which may be due to uncertainties in large-scale parameters such as the Lagrangian integral time scale T_L.

In figure 9(b), it can be seen that the model shows good agreement with DNS in $\langle u^2 \rangle^{1/2}$ overall. However, some 'wiggles' at intermediate times in the data for the two smallest initial separations are evident. This suggests that the model in the dissipation range is causing the velocity to accelerate too fast, so that the resulting Lagrangian velocity increment overshoots DNS values before it is forced to relax back into approximate inertial range behaviour. A higher-order model is probably required to improve upon this feature. However, because the separation is the time integral of the velocity, the overall separation at later times is not strongly affected by this velocity anomaly, which is essentially limited to the first 20 Kolmogorov time scales of the dispersion process.

In figure 9(c, d), it can be seen that, except perhaps for the flatness at early times, the model is capable of following the trend for the development of non-Gaussian characteristics in time. The level of quantitative agreement reached for these moments is somewhat less optimal than that achieved for the separation distance (figure 7). However, this is not surprising, since stronger intermittency in the separation speed implies greater uncertainties for higher-order moments. In DNS, the use of a finite number of particle pairs also introduces significant errors in statistical sampling. Allowing for these non-ideal factors, the agreement we demonstrate here can be considered to be quantitatively adequate.

6.3. *Separation p.d.f. and Richardson scaling*

Although knowledge of the first four moments of the separation distance is sufficient for many practical purposes, it is also useful to make comparisons for the separation p.d.f., which has long been recognized to have a fundamental role (Batchelor 1952). This p.d.f. was originally referred to by Richardson (1926) as the distance-neighbour function, and has been measured in a laboratory experiment by Ott & Mann (2000).

Figure 10 shows the separation p.d.f. at different times for $R_\lambda = 230$ and $l_0/\eta = 16$. This is the case of the highest Reynolds number and intermediate initial separation in the DNS, corresponding to optimal conditions for inertial-range behaviour. The results here can be compared with DNS data similar to those in figure 8 in Part 1, except for a different normalizing scale for the separation distance. At $t = 0$, the p.d.f. is a delta function at unity. Subsequently, it stretches out with the tails reaching very large values before eventually relaxing back to a form which corresponds to l becoming the magnitude of a vector with three independent Gaussian Cartesian components. It can be seen that these trends are captured well by the model.

While the distance-neighbour function is the p.d.f. of the particle-pair separation vector ($\boldsymbol{l}$), in isotropic turbulence it is a function, say $q(l)$, of the separation distance

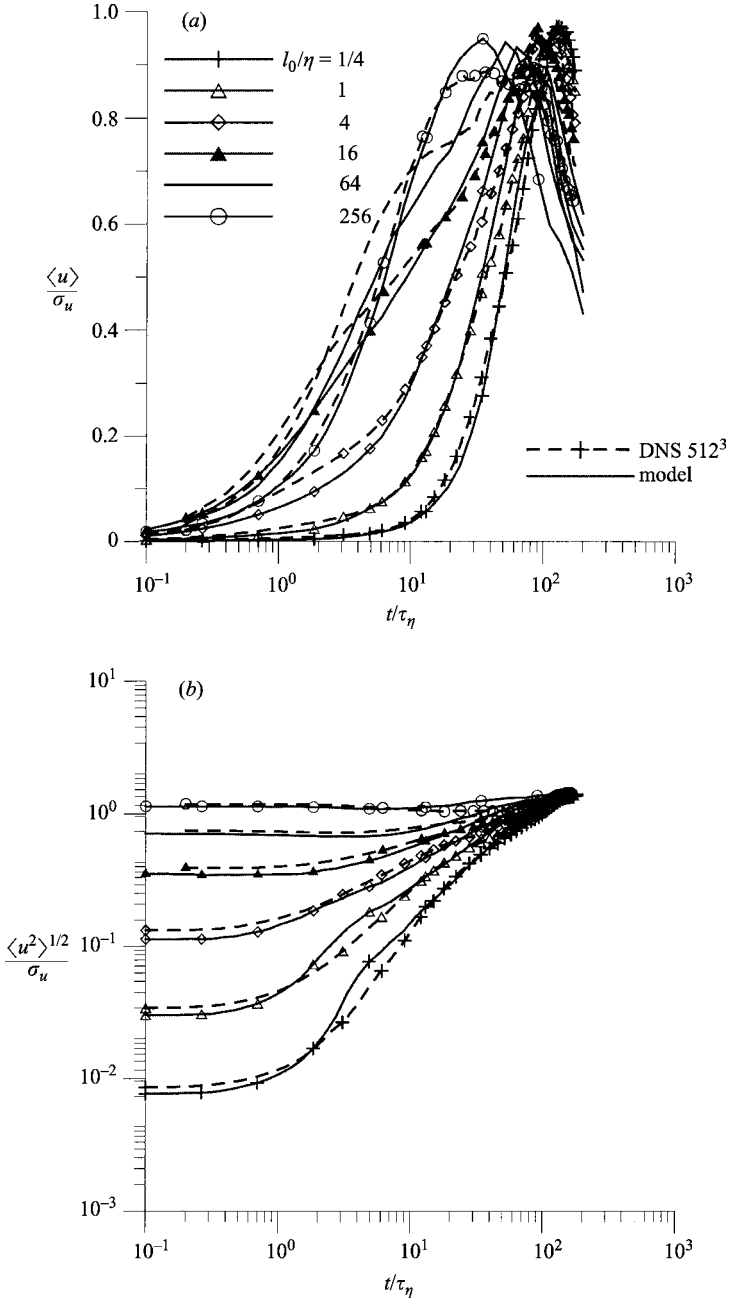

FIGURE 9(*a*, *b*). For caption see facing page.

($l = |\boldsymbol{l}|$) only. It is furthermore related to the p.d.f. of l itself by

$$P(l) = 4\pi l^2 q(l), \tag{46}$$

where the factor $4\pi l^2$ appears by virtue of integration over a spherical surface of radius l in sample space. Richardson also introduced a model for $q(l)$ in the inertial

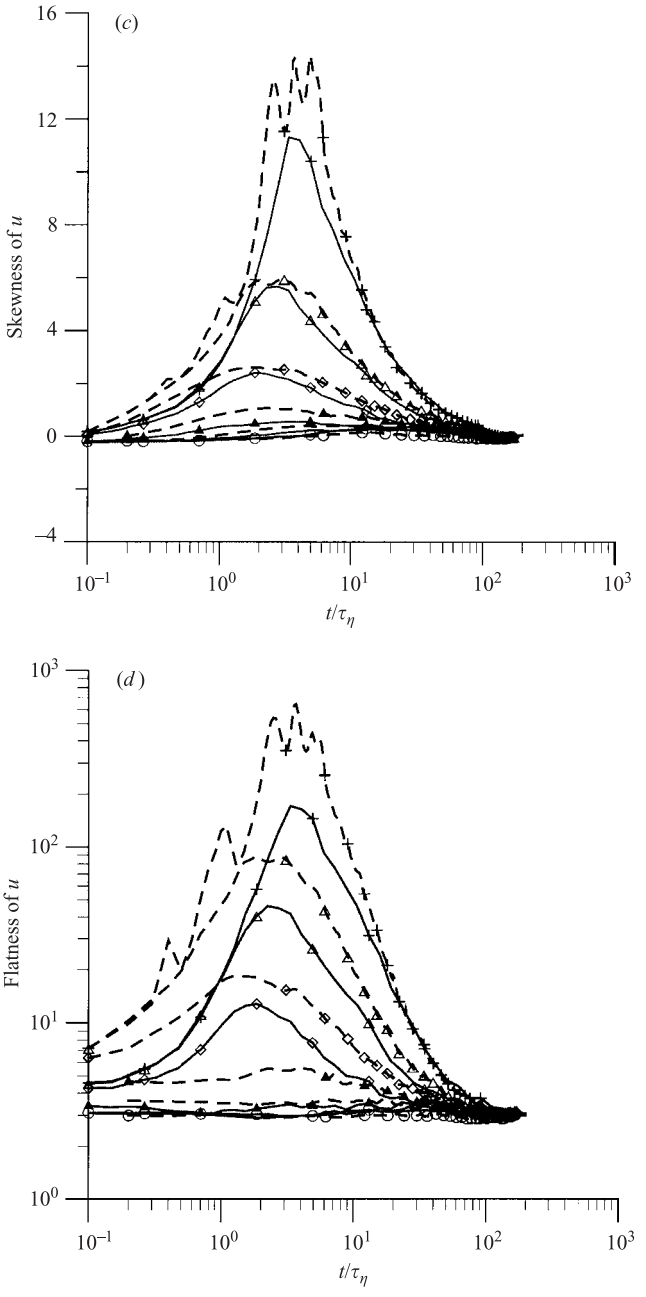

FIGURE 9. (*a*) Mean separation speed for various initial separations at $R_\lambda = 230$. Thicker lines show larger initial separations in (*a*) as indicated in the legend. (*b*) root-mean-square separation speed; (*c*) skewness of separation speed; (*d*) flatness of separation speed. Solid lines show the model results, dashed lines for the DNS.

range. It corresponds to a separation-distance p.d.f. of the form

$$P(l) = A\frac{l^2}{\langle l^2\rangle^{3/2}}\exp\left[-B\left(\frac{l^2}{\langle l^2\rangle}\right)^{1/3}\right], \tag{47}$$

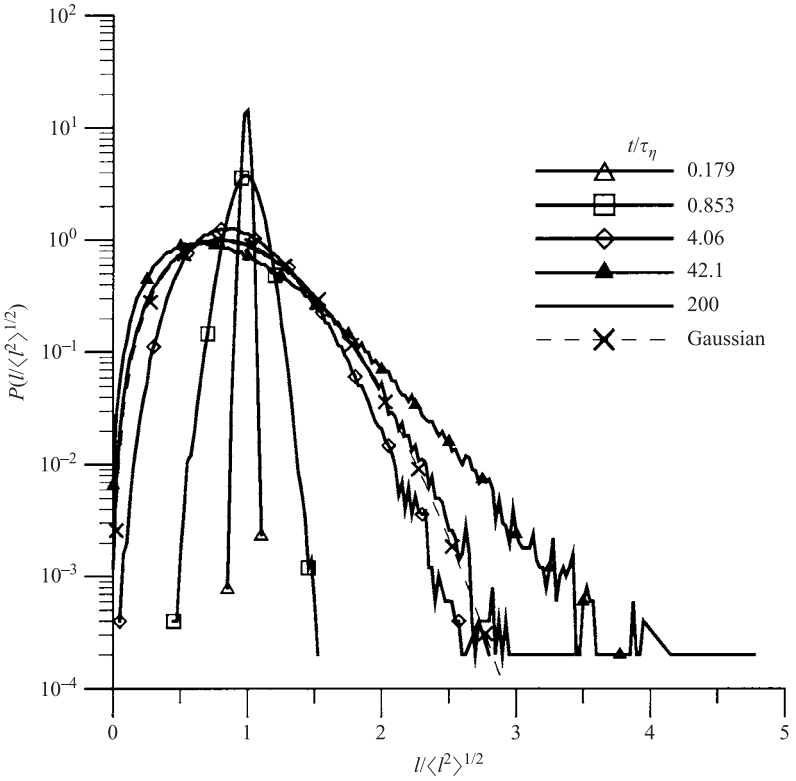

FIGURE 10. Normalized model separation p.d.f. for the initial separation $l_0/\eta = 16$ for the $R_\lambda = 230$ case and various elapsed dispersion times ranging from small (delta-function like), near inertial (stretched tails), to large time (Gaussian separations). Gaussian separations give the dashed line for the separation magnitude.

where the numerical coefficients are

$$A = \frac{32}{315}\frac{1}{\sqrt{\pi}}\left(\frac{1287}{8}\right)^{3/2}, \quad B = \left(\frac{1287}{8}\right)^{1/3}. \tag{48}$$

Remarkably, Ott & Mann (2000) have suggested that these asymptotic results are attained in experiments at a relatively modest $R_\lambda \approx 90$. The value of R_λ is the same as in Yeung (1994) (and one of the cases studied in Part 1). In our results at this R_λ, the choice of initial separation that gives the best approximation to inertial-range scaling is that of $l_0/\eta = 4$ (shown below).

Taken together, (46)–(48) suggest that a test for the Richardson form of the separation p.d.f. can be made by plotting $q(l)\langle l^2\rangle^{3/2}$ as a function of $(l^2/\langle l^2\rangle)^{1/3}$, on linear–log scales. The best match is expected to occur in a time range where, according to (3), $\langle l^2\rangle$ has at least some resemblance to t^3 behaviour. Figure 11 shows results from stochastic modelling. Note that there is a good collapse of the data close to the Richardson form, roughly in the range $0.2 \leqslant l/\langle l^2\rangle^{1/2} \leqslant 3$, with the best agreement for the intermediate elapsed dispersion time $t \approx 14\tau_\eta$. However, careful examination of figure 7(c, d) shows that, for both DNS and modelling, the skewness and flatness factors obtained in this regime are lower than those of Richardson's distribution (which can be deduced analytically from (47) and (48), as 1.70 and 7.81, respectively).

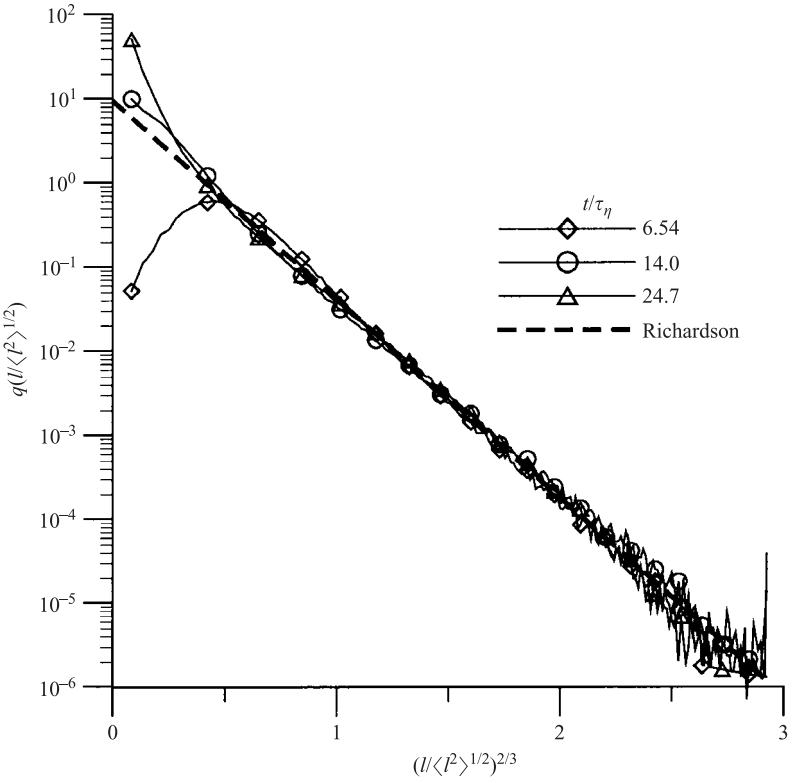

FIGURE 11. Scaled p.d.f. of separation distance in a form suitable for comparison with Richardson scaling. Model results are for $l_0/\eta = 4$ at Reynolds number $R_\lambda = 90$ for intermediate elapsed dispersion times (which fit t^3 growth of the mean square dispersion), showing collapse onto the Richardson form shown as the dashed line, (48).

A test similar to that in figure 11 was made by Ott & Mann (2000), who assumed that the mean-square separation strictly follows Richardson's scaling (3). Given the rigorous Reynolds number requirements for Kolmogorov scaling in Lagrangian statistics (Sawford 1991; Yeung 2002), the claim that (3) is attained at $R_\lambda = 90$ is somewhat surprising. One test of (3) is to plot $\langle l^2\rangle - l_0^2$ versus time, and look for t^3 growth. Figure 12 shows such a plot. The results are similar to those taken from DNS at a slightly higher Reynolds number ($R_\lambda = 283$) by Ishihara & Kaneda (2002), who also found a limited range of inertial-range-like behaviour. However, there are reasons why the results in figure 12 should not be interpreted as satisfying Richardson scaling. If there is robust t^3 inertial-range behaviour, then a plot of $\langle l^2\rangle$ at different Reynolds number should reveal collapse to the same curve as the Reynolds number increases, and this limiting curve corresponds to Richardson's form gt^3 for fixed constant g. In fact, the plots in figure 12 for $\langle l^2\rangle$ at $R_\lambda = 90$ and 230, for the same absolute initial separation (l_0), demonstrate that this is not the case. The curve for lower Reynolds number fortuitously is 'tangent' to t^3 nominally in the inertial subrange, but the separation behaviour for a higher-Reynolds-number flow with the same initial separation is nowhere near a t^3 scaling. This plot shows that the separation process is not close to an inertial-range limit. The collapse to Richardson-like scaling indicates that, at a particular Reynolds number, the process satisfies a diffusion equation,

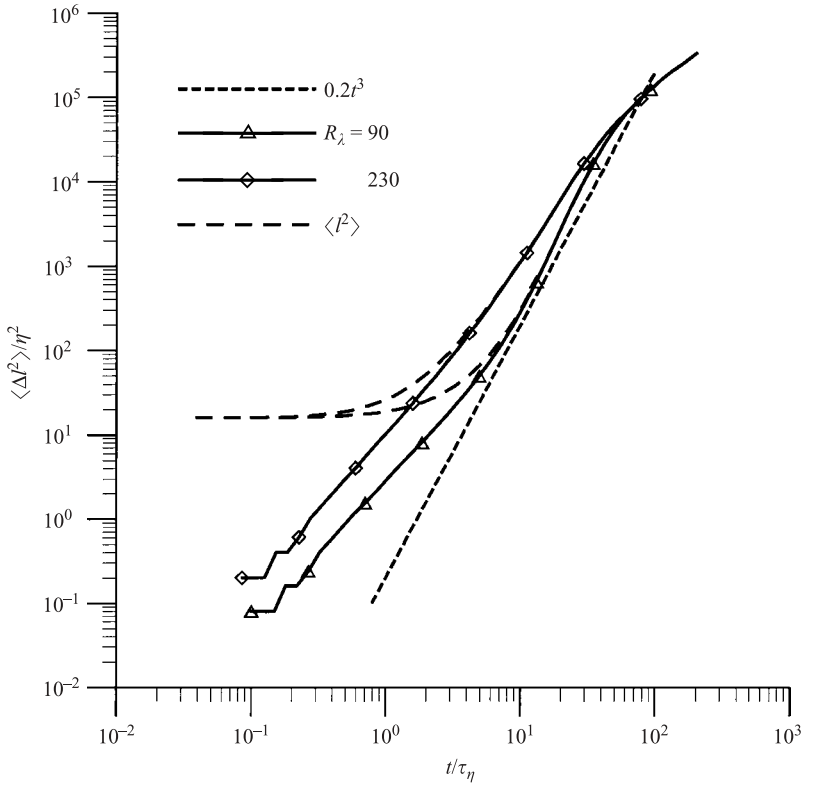

FIGURE 12. Growth of model mean-square separation with time, for initial separation $l_0/\eta = 16$ at $R_\lambda = 230$, and $l_0/\eta = 4$ at $R_\lambda = 90$ (fixed absolute l_0). Difference from initial square-separation shown as solid lines with symbols; dashed lines give the mean-square of l. Lower Reynolds-number curve approximates t^3 growth (parallel to the dashed straight line) in a spurious inertial range.

but with separation and diffusivity still depending on the initial conditions. Thus, by choosing the initial-separation parameter to give approximately t^3 mean-square relative dispersion, the overall spatial structure is also tuned to Richardson's form (3). It should also be noted (B. L. Sawford, private communication 2002) that this implies that the effects of initial separation are still strong in the scaling ranges supposedly being observed. This dependence on initial conditions is in clear violation of inertial-range arguments necessary for Richardson scaling. These reservations do not necessarily imply that the value of g given by Ott & Mann (2000) is inaccurate; but that the true value cannot be unambiguously established at the Reynolds number in the experiments (nor with current DNS).

It is useful to see how data at higher Reynolds number behave in the context of approach to Richardson scaling. Figure 13 shows the development of the separation p.d.f., at $R_\lambda = 230$. The initial separation is again four Kolmogorov scales, the value most suggestive of an inertial range in this case at higher Reynolds number. The agreement with Richardson scaling again seems outwardly reasonable. Yet, because of the lack of convergence with Reynolds number demonstrated in figure 12, we argue that this agreement is just an artefact of dissipation-range effects instead of a true indication of inertial-range scaling.

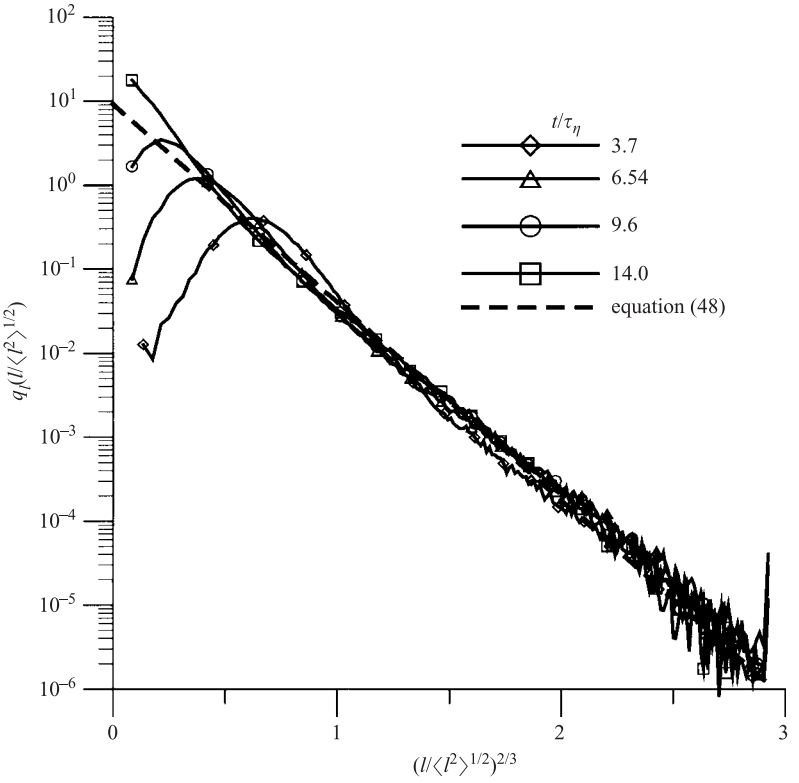

FIGURE 13. Similar to figure 11, for model results at $R_\lambda = 230$ again for the initial separation $l_0/\eta = 4$, showing a moderate degree of collapse onto the Richardson form shown as the dashed line, (48).

7. Conclusions and discussion

In this paper, we have developed and tested a new stochastic model of two-particle dispersion in isotropic turbulence, tightly coupled with the use of direct numerical simulations (Part 1). The model is quasi-one-dimensional in nature (see § 2), focusing on the magnitudes of the separation and relative velocity vectors, thereby avoiding non-uniqueness difficulties in stochastic model equations for the three-dimensional vectors. Tests of the model using Lagrangian data from DNS (presented in § 6) show that the new model is capable of mimicking behaviour encountered in turbulent relative dispersion. The new model performs substantially better than previous ones which, although adequate for low-order moments, have been criticized in the literature as being unable to reproduce strong non-Gaussianity in relative dispersion in the regime of short diffusion time and small separation (i.e. the dissipation range). One contribution of this work is a validation of the capacity of stochastic models to describe turbulent separation processes, even for difficult-to-model viscous effects.

The search for reasons behind the shortcomings of previous stochastic models has revealed several critical constraints for modelling the separation process. The first is the need to capture non-Gaussian behaviour, particularly in the tails, of the Eulerian separation-speed probability density function. An accurate functional form for this p.d.f. is necessary for the new stochastic model to be sensitive to the occurrence of large

separation speeds which correspond to infrequent but significant instances of particle pairs suddenly accelerating apart within a short time interval. A second requirement is to formulate a model consistent with two-point statistics of the acceleration conditioned upon the separation speed (Borgas & Yeung 1998). We have found that good results can be obtained by assuming a power-law fall-off in the tails for large velocities in the Eulerian separation-speed p.d.f. together with a quadratic-form model for the conditional acceleration. Essentially, these specifications allow the new model to describe the observed intermittency of the separation process in a quantitative manner, at least in the dissipation range where particle-pair separation is also subject to viscous retardation.

Substantial effort has been made (§§3–4) in providing essentially an analytical formulation of the model, so that Lagrangian dispersion results can be obtained using efficient numerical implementations (described in §5). Model results obtained with appropriately tuned model parameters are seen to provide a very good representation of relative dispersion, measured not just by the mean separation, but also by the r.m.s., skewness and flatness factors, as well as the form of the separation probability density function. The latter, in particular, is found to agree with Lagrangian data from DNS, as well as with recent laboratory measurements.

As noted in §6, the success of our stochastic model depends on tuning the values of several model parameters. This tuning is quite complex, and while not a desirable feature, it is unavoidable. However, some definite physical meaning can be assigned to at least one of the tuning parameters, namely the maximum separation speed allowed for the process at each separation length scale. This velocity (§3) is taken to be a fixed multiple of the r.m.s. value (σ). The truncation applied to this p.d.f. amounts to a simple representation for the way in which power-law tails undergo transition to a faster cutoff, such as exponential decay for a Gaussian distribution. Our motivation for adopting a simple absolute cutoff is mainly for practical expediency, since the details of a smooth transition in shape for the tails of the p.d.f. are difficult to implement. Nevertheless, the chosen values for this Eulerian cutoff parameter seem to work well, and have played an important role in allowing the Lagrangian model to capture the extreme non-Gaussian behaviour. As indicated earlier, the present treatment of the p.d.f. tails is a major improvement over previous models.

Accurate modelling of the dissipation range is essential in this work, because viscous effects play a substantial role in issues of Reynolds-number dependence. The latter is, in turn, important because while practical applications are often at very high Reynolds number, the most reliable and detailed sources of Lagrangian data are direct numerical simulations at moderate Reynolds number. A recent example of the use of DNS for stochastic modelling, for single-particle statistics in homogeneous turbulent shear flow, is provided by Sawford & Yeung (2000, 2001). It is reasonable to expect that successful performance of stochastic models in the current Reynolds-number range of DNS will give greater confidence in their performance in inertial-range turbulence where they are formally more suited. Successful treatment of viscous effects in this work also suggests that the new modelling approach can be extended to describe the motion of material fluid particles subject to molecular diffusion (Saffman 1960).

Because Lagrangian inertial-range similarity requires higher Reynolds numbers than for Eulerian quantities, the procedure for extrapolating our new stochastic model to arbitrarily large Reynolds number is uncertain. Nevertheless, this work can be taken as a validation of the stochastic-model approach for describing Lagrangian statistics in turbulent flow. We now have greater confidence that such models work for ever larger Reynolds number, and for inertial-range processes in particular. Many of the concepts

developed here to model viscous effects, including realizability constraints and detailed parameterization of the conditional acceleration in the p.d.f. transport equation, are expected to be useful for stochastic modelling in other contexts. One example of these would, for instance, be single-particle dispersion in the near-wall region of the atmospheric surface layer. Our work in the present paper has demonstrated that it is important to have an accurate understanding, either from DNS or experiments, of the tails of the p.d.f. of Eulerian velocity increments, which depend on the spatial structure of the flow.

The authors gratefully acknowledge support from the National Science Foundation (NSF, Grant no. INT-9526868) and the Australian Government Department of Industry, Science and Technology (International Bilateral Exchange Program no. 95/4358) which have made our collaboration possible. We also thank Brian L. Sawford for his encouragement and his comments on an early version of the manuscript.

Appendix. Eulerian structure functions

Here we give the details of parameterized functional forms for Eulerian velocity structure functions up to the fourth order. These can also be viewed as interpolation formulae covering all values of spatial separation in ways consistent with asymptotic ranges implied in (11) and (12).

To begin, we always assume that

$$\overline{\epsilon} = \frac{\sigma_u^3}{L}, \quad \eta = \left(\frac{\nu^3}{\overline{\epsilon}}\right)^{1/4} \tag{A 1}$$

and that the first moment is trivial with

$$\langle \Delta_r u \rangle = 0. \tag{A 2}$$

For the second moment, we use the parameterization

$$\langle (\Delta_r u)^2 \rangle = 2\sigma_u^2 \left(1 - \exp\left(-\frac{\alpha_2 l}{\eta}\right)\right)^{4/3} \left(\frac{l^4}{\beta_2 L^4 + l^4}\right)^{1/6}. \tag{A 3}$$

Notice that for large separations,

$$\langle (\Delta_r u)^2 \rangle = 2\sigma_u^2 \left(1 - \frac{L^4}{6\beta_2} l^{-4}\right), \tag{A 4}$$

which ensures a valid spectrum for this velocity field. In the dissipation subrange

$$\langle (\Delta_r u)^2 \rangle \sim \langle s^2 \rangle l^2 = \frac{1}{15}\frac{\overline{\epsilon}}{\nu} l^2 \sim 2\sigma_u^2 \left(\frac{\alpha_2}{\eta}\right)^{4/3} \left(\frac{1}{\beta_2 L^4}\right)^{1/6} l^2, \tag{A 5}$$

then

$$\frac{1}{15}\frac{\overline{\epsilon}}{\nu} = 2\frac{\sigma_u^2}{L^{2/3}} \alpha_2^{4/3} \eta^{-4/3} \beta_2^{-1/6} = 2\left(\frac{\sigma_u^3}{L}\right)^{2/3} \left(\frac{\nu^3}{\overline{\epsilon}}\right)^{-1/3} \alpha_2^{4/3} \beta_2^{-1/6} \Rightarrow \alpha_2^{-4/3} \beta_2^{1/6} = 30. \tag{A 6}$$

The dissipation range effects fall off exponentially fast for large values of l/η, leaving the inertial subrange:

$$\langle (\Delta_r u)^2 \rangle \sim C_{Kol} (\overline{\epsilon} l)^{2/3} 2\sigma_u^2 \left(\frac{1}{\beta_2 L^4}\right)^{1/6} l^{2/3} \sim 2\beta_2^{-1/6} (\overline{\epsilon} l)^{2/3} \Rightarrow 2\beta_2^{-1/6} = C_{Kol}, \tag{A 7}$$

$$\alpha_2^{-4/3} = 15 C_{Kol}. \tag{A 8}$$

Similarly, for the third moment we have

$$\langle(\Delta_r u)^3\rangle = \langle(\Delta_r u)^2\rangle^{3/2}\left((S - S_0)\exp(-\alpha_3 l/\eta) + S\frac{\beta_3 L^4}{\beta_3 L^4 + l^4}\right), \tag{A 9}$$

with the dissipation and inertial-range values, respectively,

$$S_0 = -0.55, \quad S = -\tfrac{4}{5}C_{Kol}^{-3/2}. \tag{A 10}$$

For the fourth moment

$$\langle(\Delta_r u)^4\rangle = \langle(\Delta_r u)^2\rangle^2\left(3 + (F_0 - F)\exp(-\alpha_4 l/\eta) + (F - 3)\frac{\beta_4 L^4}{\beta_4 L^4 + l^4}\right), \tag{A 11}$$

with dissipation range values

$$F_0 = 6 + 4(R_\lambda - 38)/202, \tag{A 12}$$

and the inertial range value $F = 3.2$.

REFERENCES

Anselmet, F., Gagne, Y., Hopfinger, E. & Antonia, R. A. 1984 High-order velocity structure functions in turbulent shear flows. *J. Fluid Mech.* **140**, 63–89.

Batchelor, G. K. 1952 Diffusion in a field of homogeneous turbulence. II. The relative motion of particles. *Proc. Camb. Phil. Soc.* **48**, 345–362.

Borgas, M. S. & Sawford, B. L. 1991 The small-scale structure of acceleration correlations and its role in the statistical theory of turbulent dispersion. *J. Fluid Mech.* **228**, 295–320.

Borgas, M. S. & Sawford, B. L. 1994*a* A family of stochastic models for two-particle dispersion in isotropic homogeneous stationary turbulence. *J. Fluid Mech.* **279**, 69–99.

Borgas, M. S. & Sawford, B. L. 1994*b* Stochastic equations with multifractal random increments for modelling turbulent dispersion. *Phys. Fluids* **6**, 618–632.

Borgas, M. S. & Sawford, B. L. 1996 Molecular diffusion and viscous effects on concentration statistics in grid turbulence. *J. Fluid Mech.* **324**, 25–54.

Borgas, M. S. & Yeung, P. K. 2001 Particle pair separation processes in turbulence. *14th Australasian Fluid Mech. Conf. Adelaide University, Adelaide, Australia*, 10–14 December 2001, vol. 1, 171–173.

Borgas, M. S. & Yeung, P. K. 1998 Conditional fluid-particle accelerations in turbulence. *Theoret. Comput. Fluid Dyn.* **11**, 69–93.

Durbin, P. A. 1980 A stochastic model of two-particle dispersion and concentration fluctuations in homogeneous turbulence. *J. Fluid Mech.* **100**, 279–302.

Durbin, P. A. 1982 Analysis of the decay of temperature fluctuations in isotropic turbulence. *Phys. Fluids* **25**, 1328–1332.

Flohr, P. & Vassilicos, J. C. 2000 Scalar subgrid model with flow structure for large-eddy simulation of scalar variances. *J. Fluid Mech.* **407**, 315–349.

Franzese, P. & Borgas, M. S. 2002 A simple relative dispersion model for concentration fluctuations in contaminant clouds. *J. Appl. Met.* **41**, 1101–1111.

Frisch, U. 1995 *Turbulence: the Legacy of A. N. Kolmogorov*. Cambridge University Press.

Fung, J. C. H., Hunt, J. C. R., Malik, N. A. & Perkins, R. J. 1992 Kinematic simulation of homogeneous turbulence by unsteady random Fourier modes. *J. Fluid Mech.* **236**, 281–318.

Gardiner, C. W. 1985 *Handbook of Stochastic Methods for Physics, Chemistry and the Natural Sciences*. Springer.

Girimaji, S. S. & Pope, S. B. 1990 Material element deformation in isotropic turbulence. *J. Fluid Mech.* **220**, 427–458.

Gradshteyn, I. S. & Ryzhik, I. M. 1980 *Table of Integrals, Series, and Products*. Academic.

Heppe, B. M. O. 1998 Generalized Langevin equation for relative turbulent dispersion. *J. Fluid Mech.* **357**, 167–198.

Ishihara, T. & Kaneda, Y. 2002 Relative diffusion of a pair of fluid particles in the inertial subrange of turbulence. *Phys. Fluids* **14**, L69–L72.

JIMENEZ, J. 1998 Turbulent velocity fluctuations need not be Gaussian. *J. Fluid Mech.* **376**, 139–147.

KENDALL, M. G. & STUART, A. 1969 *The Advanced Theory of Statistics. Vol. 1: Distributions*, 3rd edn. Charles Griffin, London, UK.

KURBANMURADOV, O. A. 1995 A new Lagrangian model of two-particle relative turbulent dispersion. *Monte Carlo Meth. Appl.* **1**, 83–100.

KURBANMURADOV, O. A. 1997 Stochastic Lagrangian models for two-particle relative dispersion in high-Reynolds number turbulence. *Monte Carlo Meth. Appl.* **3**, 37–52.

KURBANMURADOV, O. A. & SABELFELD, K. K. 1995 Stochastic Lagrangian models of relative dispersion of a pair of fluid particles in turbulent flows. *Monte Carlo Meth. Appl.* **1**, 101–136.

LEWIS, D. M. & PEDLEY, T. J. 2000 Planktonic contact rates in homogeneous isotropic turbulence: theoretical predictions and kinematic simulations. *J. Theoret. Biol.* **205**, 377–408.

LUHAR, A. K., HIBBERD, M. F. & BORGAS, M. S. 2000 A skewed meandering-plume model for concentration statistics in the convective boundary layer. *Atmos. Environ.* **34**, 3599–3616.

MALIK, N. A. & VASSILICOS, J. C. 1999 A Lagrangian model for turbulent dispersion with turbulent-like flow structure: comparison with direct numerical simulation for two-particle statistics. *Phys. Fluids* **11**, 1572–1580.

MONIN, A. S. & YAGLOM, A. M. 1975 *Statistical Fluid Mechanics*, vol. 2, MIT Press.

OBUKHOV, O. M. 1941*a* Spectral energy distribution in a turbulent flow. *Dokl. Akad. Nauk SSSR*, **32**, 22–24.

OBUKHOV, O. M. 1941*b* Spectral energy distribution in a turbulent flow. *Izv. Akad. Nauk SSSR Georgr. i Geofiz.* **5**, 453–456.

OTT, S. & MANN, J. 2000 An experimental investigation of the relative diffusion of particle pairs in three-dimensional turbulent flow. *J. Fluid Mech.* **422**, 207–223.

PEDRIZZETTI 1999 Quadratic Markov modelling for intermittent turbulence. *Phys. Fluids* **11**, 1694–1696.

PEDRIZZETTI, G. & NOVIKOV, E. A. 1994 On Markov modelling of turbulence. *J. Fluid Mech.* **280**, 69–93.

POPE, S. B. 1994 Lagrangian pdf methods for turbulent flows. *Annu. Rev. Fluid Mech.* **26**, 23–63.

POPE, S. B. 2000 *Turbulent Flows*. Cambridge University Press.

REYNOLDS, A. M. 1999 The relative dispersion of particle pairs in stationary homogeneous turbulence. *J. Appl. Met.* **38**, 1384–1390.

RICHARDSON, L. F. 1926 Atmospheric diffusion shown on a distance-neighbour graph. *Proc. R. Soc. Lond.* A **110**, 709–737.

SAFFMAN, P. G. 1960 On the effect of molecular diffusivity in turbulent diffusion. *J. Fluid Mech.* **8**, 273–283.

SAWFORD, B. L. 1985 Lagrangian statistical simulation of concentration mean and fluctuating fields. *J. Clim. Appl. Met.* **24**, 1152–1166.

SAWFORD, B. L. 1991 Reynolds number effects in Lagrangian stochastic models of dispersion. *Phys. Fluids* A **3**, 1577–1586.

SAWFORD, B. L. 2001 Turbulent relative dispersion. *Annu. Rev. Fluid Mech.* **33**, 289–317.

SAWFORD, B. L. & BORGAS, M. S. 1994 On the continuity of stochastic models for the Lagrangian velocity in turbulence. *Physica* D **76**, 297–311.

SAWFORD, B. L. & YEUNG, P. K. 2000 Eulerian acceleration statistics as a discriminator between Lagrangian stochastic models in uniform shear flow. *Phys. Fluids* **12**, 2033–2045.

SAWFORD, B. L. & YEUNG, P. K. 2001 Lagrangian statistics in uniform shear flow: DNS and stochastic models. *Phys. Fluids* **13**, 2627–2634.

SORNETTE, D. 2000 *Critical Phenomena in Natural Sciences: Chaos, Fractals, Self-Organisation and Disorder: Concepts and Tools*. Springer.

SREENIVASAN, K. R. 1995 On the universality of the Kolmogorov constant. *Phys. Fluids* **7**, 2778–2784.

SREENIVASAN, K. R. 1998 An update on the dissipation rate in isotropic turbulence. *Phys. Fluids* **10**, 528–529.

SREENIVASAN, K. R. & ANTONIA, R. A. 1997 The phenomenology of small-scale turbulence. *Annu. Rev. Fluid Mech.* **29**, 435–472.

TAYLOR, G. I. 1921 Diffusion by continuous movements. *Proc. Lond. Math. Soc. ser.* 2, **20**, 196–212.

THOMSON, D. J. 1987 Criteria for the selection of stochastic models of particle trajectories in turbulent flows. *J. Fluid Mech.* **180**, 529–556.

Thomson, D. J. 1990 A stochastic model for the motion of particle pairs in isotropic high-Reynolds-number turbulence, and its application to the problem of concentration variance. *J. Fluid Mech.* **210**, 113–153.

Yeung, P. K. 1994 Direct numerical simulation of two-particle relative diffusion in isotropic turbulence. *Phys. Fluids* **6**, 3416–3428.

Yeung, P. K. 2002 Lagrangian investigations of turbulence. *Annu. Rev. Fluid Mech.* **34**, 115–142.

Yeung, P. K. & Borgas, M. S. 1998 Vector alignment properties of particle-pair dispersion in isotropic turbulence. *13th Australasian Fluid Mech. Con. Monash University, Melbourne, Australia*, 13–18 December 1998, vol. 2, 729–732.

Yeung, P. K. & Borgas, M. S. 2004 Relative dispersion in isotropic turbulence. Part 1. Direct numerical simulations and Reynolds number dependence. *J. Fluid Mech.* **503**, 93–124.

Yeung, P. K. & Pope, S. B. 1989 Lagrangian statistics from direct numerical simulations of isotropic turbulence. *J. Fluid Mech.* **207**, 531–586.

Yeung, P. K. & Zhou, Y. 1997 On the universality of the Kolmogorov constant in numerical simulations of turbulence. *Phys. Rev.* E **56**, 1746–1752.